Energy Engineering

Tech Science Press

https://doi.org/10.32604/ee.2026.087000

ARTICLE

Assessment of Energy Self-Consumption and Potential Participation in Renewable Energy Community through a 3 kWp Photovoltaic System: Case Study of a Condominium Apartment

Giuliana Daniela Foti[1,*], Alexandra Catalina Lazaroiu[2] and Mariacristina Roscia[1]

[1]Department of Engineering and Applied Sciences, University of Bergamo, Dalmine, Italy
[2]Department of Electrical Engineering, National University of Science and Technology POLITEHNICA Bucharest, Bucharest, Romania

*Corresponding Author: Giuliana Daniela Foti. Email: giuliana.foti@unibg.it

Received: 09 June 2026; Accepted: 12 August 2026; Published: 12 November 2026

ABSTRACT: Residential photovoltaic (PV) systems can reduce grid dependence and support renewable-energy sharing within Renewable Energy Communities (RECs). However, their effectiveness in condominium buildings is often constrained by the temporal mismatch between electricity generation and demand, seasonal variability, local shading, and limited installation space. This study evaluates the technical feasibility of a 3 kWp PV system serving a condominium apartment in Peschiera Borromeo, Italy, with the objectives of improving energy performance, increasing self-consumption and self-sufficiency, and assessing the potential contribution of surplus renewable electricity to a REC. Unlike studies focusing exclusively on building retrofit, photovoltaic performance, or energy sharing, this work integrates energy-efficiency measures, site-specific PV assessment, hourly electricity-demand modeling, battery-storage operation, and REC participation within a single apartment-scale framework. An energy diagnosis was conducted to identify effective envelope and system retrofit solutions, and five electricity-demand scenarios were developed by combining heating, cooling, domestic hot-water production, and household-appliance loads. PV generation was estimated using PVGIS and an independent site-specific hourly analytical model accounting for solar geometry, module temperature, and local shading. The best retrofit configuration improved the apartment's energy rating from class F to A3 and reduced primary energy demand by 82.05%. Annual PV generation was estimated at 4022.01 kWh by PVGIS and 3671.38 kWh by the analytical model. With a 5 kWh battery, the highest self-consumption and self-sufficiency rates reached 78.64% and 77.33%, respectively, while the most efficient complete-demand scenario achieved 72.99% self-sufficiency. PV generation fully covered monthly electricity demand in July and August, whereas grid dependence remained significant during winter because of reduced solar availability and higher thermal loads. The results demonstrate that the proposed configuration can substantially reduce grid withdrawals and generate renewable-electricity surpluses suitable for collective self-consumption within a REC, although PV integration alone cannot ensure year-round energy independence.

KEYWORDS: Residential photovoltaic systems; building energy retrofit; self-consumption; energy self-sufficiency; battery energy storage; renewable energy communities (RECs); shading assessment; condominium buildings

1 Introduction

The decarbonization of the residential sector is a key element of the transition toward sustainable, decentralized, and resilient energy systems. In this context, photovoltaic (PV) technologies have become one of the most effective solutions for increasing renewable electricity generation at the building scale,

Copyright © 2027 The Authors. Published by Tech Science Press. This work is licensed under a Creative Commons Attribution 4.0 International License, which permits unrestricted use, distribution, and reproduction in any medium, provided the original work is properly cited.

reducing dependence on centralized energy supply, and promoting distributed self-consumption models [1–6]. However, the performance of residential PV systems depends not only on the amount of electricity generated but also on its temporal match with household demand, which determines the actual utilization of locally produced renewable energy.

For this reason, the analysis of self-consumption and self-sufficiency has become central in residential energy research. The comparison between electricity generation and consumption profiles allows the assessment of key indicators such as self-consumption, demand coverage, grid imports and exports, and the contribution of battery energy storage systems [4,5,7]. These indicators provide valuable information on the interaction between household demand, local renewable generation, storage technologies, and the electricity grid.

Such analyses are particularly relevant within RECs, where locally generated renewable electricity can be shared among multiple users [8–11]. In this framework, residential consumers become prosumers, contributing not only to their own energy needs but also to the collective energy balance. Consequently, the value of residential PV systems depends on both the quantity and the timing of surplus electricity available for community sharing.

The issue is especially significant in condominium buildings, where PV deployment is often limited by roof availability, ownership arrangements, architectural constraints, and local shading conditions [1,2,4,11,12]. These factors require a careful assessment of the relationship between electricity demand, renewable generation potential, storage capacity, and opportunities for collective energy sharing.

Although previous studies have investigated PV self-consumption and battery-storage performance in residential applications, fewer contributions have combined building energy diagnosis, retrofit scenarios, site-specific PV modeling, storage assessment, and REC-oriented surplus-energy analysis within a unified framework. This integrated perspective is particularly relevant for condominium dwellings, where technical constraints and seasonal demand variability strongly affect the benefits achievable through distributed renewable-energy systems.

To address this gap, this study analyzes a condominium apartment located in Peschiera Borromeo (Milan, Italy), previously characterized through a detailed energy diagnosis. Based on this assessment, five electricity-demand scenarios were developed, representing different combinations of envelope retrofits, system efficiencies, electrification levels, and household energy uses. A 3 kWp photovoltaic system was then evaluated using both PVGIS data and an analytical model accounting for solar geometry, module temperature, and shading effects from a nearby obstacle. The resulting generation profiles were compared with the demand scenarios to assess energy balances, self-consumption, self-sufficiency, grid exchanges, and battery-storage operation, considering configurations with and without a 5 kWh battery.

The objectives of the study are: (i) to evaluate how alternative retrofit and demand scenarios affect the capability of a residential PV system to meet household electricity needs, and (ii) to quantify the amount and seasonal distribution of surplus renewable electricity potentially available for sharing within an REC.

The main contribution of this work is the development of an integrated apartment-scale framework that combines energy diagnosis, retrofit analysis, demand reconstruction, site-specific PV modeling, battery-storage evaluation, and REC-oriented surplus-energy assessment. The proposed methodology provides a practical tool for assessing residential PV performance and the potential contribution of condominium dwellings to collective renewable-energy sharing schemes under real-world constraints.

2 Case Study: Baseline Energy Performance and Retrofit Packages

The present case study emphasizes the importance of taking a comprehensive approach to enhancing residential energy efficiency. This approach involves optimizing building systems with carefully selected energy efficiency measures and monitoring and controlling household energy consumption. This methodology was applied into a condominium apartment occupied inhabited by three people. It is located on the first floor of a residential complex in Peschiera Borromeo, Milan, Italy, as shown in Fig. 1.



Figure 1: Condominium with the location of the apartment marked in red.

The apartment was constructed in the early 2000s and is located on a floor shared with two other units. An unheated garage is situated below the apartment, while heated residential units are located above. The apartment has three rooms with external walls made of hollow clay brick blocks that incorporate thermal insulation and an air cavity. The exterior of the walls is finished with exposed brickwork. The internal partition walls are made of perforated clay brick blocks. The floor slabs consist of brick-and-concrete structures that separate conditioned spaces, as well as predalle slabs that separate conditioned and unconditioned areas. The windows are fitted with standard double-glazed units in wooden frames. The apartment is served by a conventional space-heating system consisting of a natural gas boiler and cast-iron radiators for heat distribution, as shown in Fig. 2.

2.1 Energy Performance of the Retrofit Scenarios

A dynamic energy assessment was conducted using Termolog software [13] to evaluate the energy performance of the case-study apartment. The building model was developed using the Certifier module in accordance with Italian Law 90/2013 requirements. The simulation considered the main factors affecting building energy performance, such as thermal zoning, thermal bridges, solar and internal heat gains, solar shading effects, indoor temperature setpoints, and natural ventilation rates. Energy calculations were performed according to UNI/TS 11300-1:2014, D.P.R. 412/1993, UNI EN ISO 12831:2006, and UNI EN ISO 10211:2008.

The energy audit classified the apartment as Energy Class F, with a global energy performance index (EP_{gl}) of 231.13 kWh/m²·year. This result is primarily attributable to heat losses through both opaque and transparent envelope components, as well as losses associated with natural ventilation and thermal bridges. The energy classification was determined using the updated rating scale implemented in the Termolog software, based on the draft revision of the Italian Minimum Requirements Decree under discussion in 2024. Although this feature anticipated the forthcoming Energy Performance Certificate (EPC) framework, the legally applicable regulatory reference at the time of the analysis remained the Ministerial Decree of 26 June 2015.

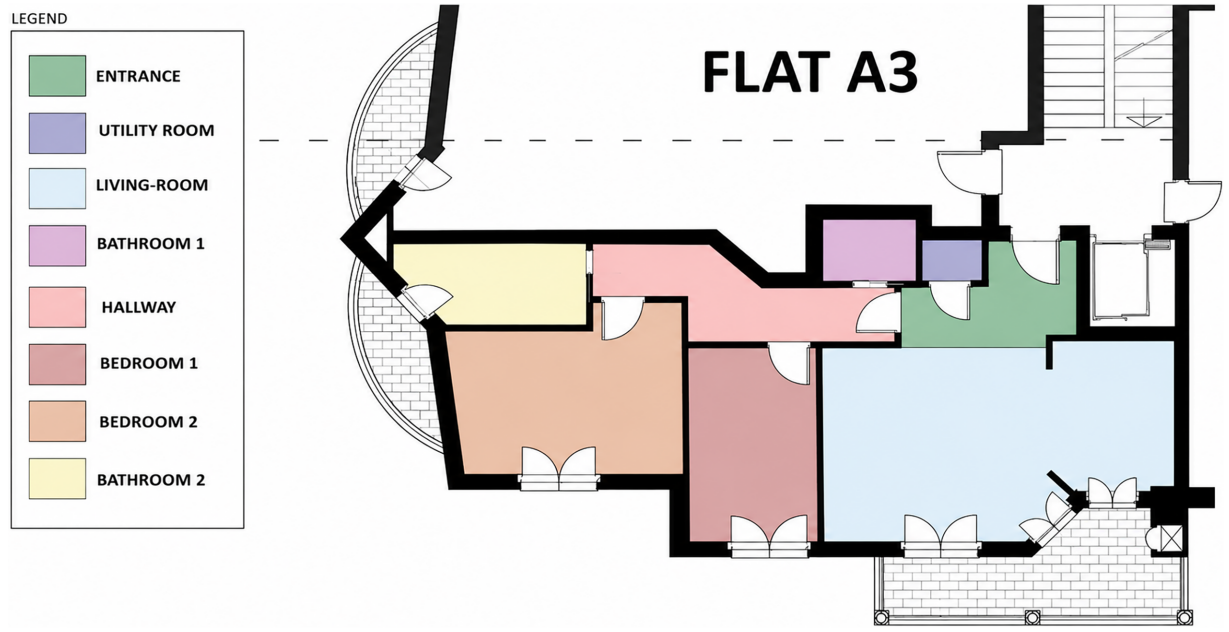


Figure 2: Scaled floor plan of the case-study apartment (1:100).

To investigate potential improvements in energy performance, several retrofit scenarios were developed and simulated using the Diagnostics module of the same software.

Fig. 3 summarizes the composition and characteristics of the retrofit packages. This methodology allowed us to compare the proposed interventions in terms of energy savings, cost-effectiveness, and overall impact on the apartment's energy performance. This comparison helped us identify the most suitable solutions for enhancing the apartment's efficiency.

The proposed measures were organized into individual and combined retrofit packages, including building envelope upgrades (**Packages A and B**) and the installation of a 3 kWp photovoltaic (PV) system (**Package F**). Further details on the PV system design and operating characteristics are provided in Section 4.

The simulated electricity generation of Package F was compared with the annual energy demand of each retrofit scenario. The latter was calculated using the EP_{gl} values obtained from the Termolog simulations and the apartment's conditioned floor area of 75.86 m^2.

First, building-envelope retrofit measures were evaluated to reduce heat losses and comply with the thermal transmittance limits applicable to Climate Zone E.

Package A involved the internal insulation of the opaque envelope and was designed to achieve a maximum thermal transmittance of 0.26 W/(m^2·K). CAM-compliant materials with appropriate thermal conductivity and thickness were considered, including high-performance Vacuum Insulating Panels (VIPs). This intervention reduced the EP_{gl} to 207.70 kWh/m^2·year, corresponding to an estimated annual energy demand of approximately 15,756 kWh, and achieved energy savings of 10.14%.

Package B addressed the transparent envelope by replacing windows and glazed components, aiming for a thermal transmittance of 1.40 W/(m^2·K). Alternative solutions were evaluated based on the type of frame and glazing while maintaining the architectural appearance of the condominium façade. The resulting configuration achieved an EP_{gl} of 193.21 kWh/m^2·year, equivalent to an annual energy demand of approximately 14,658 kWh, representing a 16.41% energy savings.

Three system retrofit strategies were investigated: replacement of the existing heat generator, integration of electric technologies into the existing system, and full electrification [1,2,13]. In **Package C**, the conventional boiler was replaced with a high-efficiency condensing unit equipped with exhaust-gas heat recovery. The retrofit reduced the annual energy demand to approximately 12,286 kWh, corresponding to an EP_{gl} of 161.96 kWh/m^2·year, and achieved energy savings of 29.93%.

Package D introduced a hybrid system consisting of a 5 kW air-to-air heat pump and three indoor units for space heating, cooling, and dehumidification. The retrofit reduced the annual energy demand to approximately 9324 kWh and lowered the EP_{gl} to 122.90 kWh/m^2·year, resulting in 46.83% energy savings relative to the baseline condition.

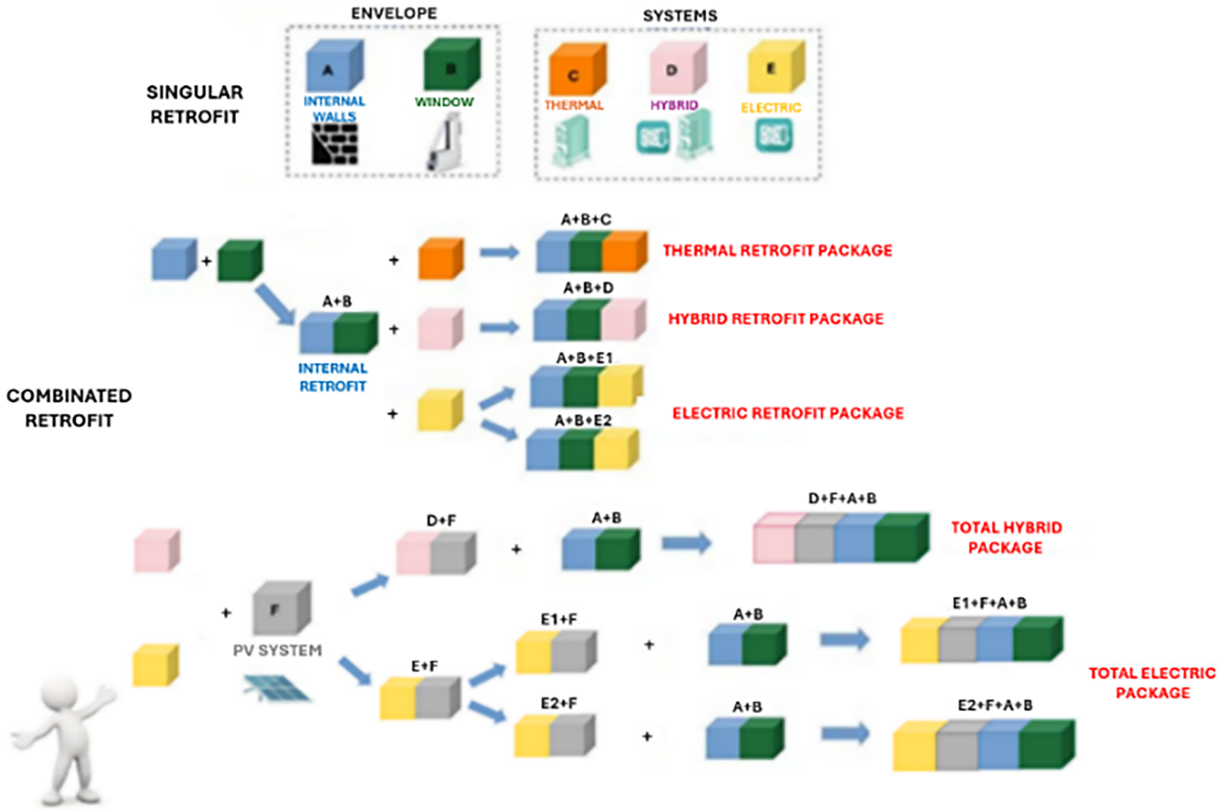


Figure 3: Energy efficiency improvement measures for assessing the energy performance of the case study.

Two all-electric configurations were also evaluated. **Package E1** included a 5 kW air-to-water heat pump, a 166-L domestic hot water storage tank, and an air-to-air heat pump for space conditioning. This configuration reduced the annual energy demand to approximately 7098 kWh, with an EP_{gl} of 93.56 kWh/m^2·year, resulting in 59.52% energy savings.

Of the individual retrofit options, **Package E2** provided the best performance. This configuration, consisting of a 2 kW electric storage water heater coupled with an air-to-air heat pump, reduced the annual energy demand to approximately 5894 kWh. It achieved an EP_{gl} of 77.68 kWh/m^2·year, corresponding to 66.39% energy savings.

A comparison of the individual retrofit scenarios shows that system upgrades generally provide greater improvements in energy performance than envelope-only measures. The combined retrofit of the opaque and transparent building envelope, represented by **Packages A+B**, improved the apartment's energy class from F

to E and resulted in energy savings ranging from 18.52% to 27.09%, depending on the selected configuration. However, heating-system upgrades alone achieved slightly higher energy savings while reaching the same energy class.

The combined analysis also confirmed the strong interaction between envelope performance and system efficiency. **Adding Packages A+B to Package E2** increased total energy savings to 69.21%, although the energy class remained unchanged. In contrast, the **A+B+E1 configuration** improved the apartment's energy class from C to A2 and achieved energy savings of 72.91%, making it the best-performing solution among the configurations without photovoltaic generation.

As illustrated in Fig. 4a,b, the integration of photovoltaic generation further enhanced the effectiveness of the retrofit measures. Among the configurations without envelope refurbishment, the **E2+F solution** delivered the best performance, reaching Energy Class A2 and achieving energy savings of 74.44%. When **Packages A+B** were combined with the system retrofit measures, energy performance improved further. In particular, the **A+B+E1+F configuration** achieved the best overall result, reaching Energy Class A3 and the highest energy savings at 82.05%.

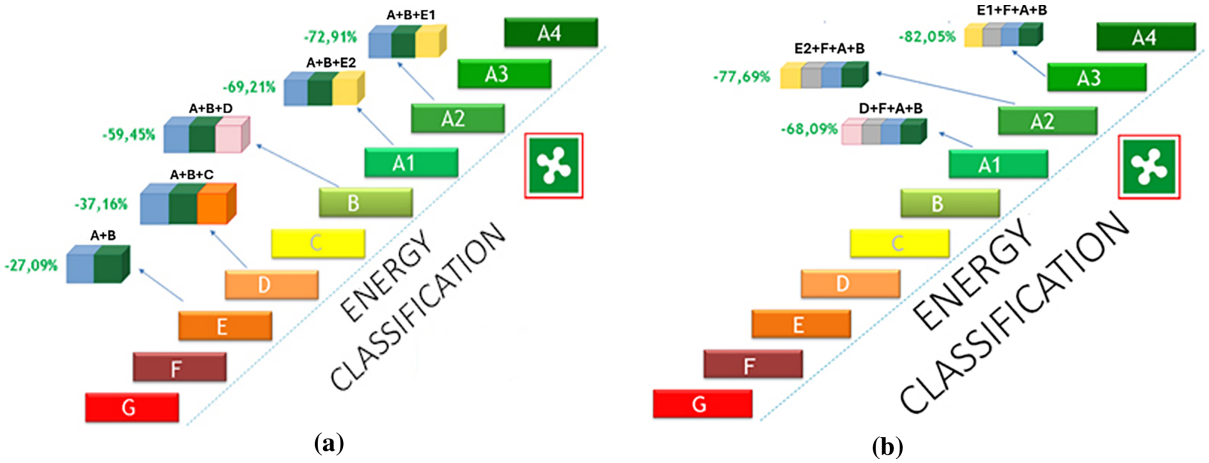


Figure 4: Energy-class progression and corresponding energy savings for the selected retrofit configurations. (**a**) Results obtained by combining the envelope retrofit measures (Packages A+B) with the heating-system upgrades. (**b**) Results obtained by integrating the PV system (Package F) with selected heating-system retrofit configurations, both with and without the envelope retrofit measures (Packages A+B).

These findings indicate that the most effective retrofit strategy combines building-envelope improvements, high-efficiency electrified heating systems, and on-site photovoltaic generation.

2.2 Definition of the Electricity-Demand Scenarios

Based on the results shown in Fig. 4a,b, five electricity-demand scenarios were defined to represent progressively more comprehensive operating conditions for the case-study apartment. The scenarios were developed assuming the actual occupancy of the dwelling, consisting of two adults and one teenager. To ensure comparability, the same occupancy conditions and appliance-use assumptions were maintained across all scenarios. Two PV-integrated retrofit configurations were selected as reference cases.

Scenario A was derived from the E2+F configuration, which represented the best-performing solution among the retrofit options without building-envelope refurbishment. It therefore describes a less invasive renovation pathway based on the electrification of building services and on-site photovoltaic generation.

Scenario B was derived from the A+B+E1+F configuration, which achieved the highest overall energy performance and represents a comprehensive retrofit strategy combining improvements to the opaque and transparent envelope, high-efficiency electric systems, and photovoltaic generation.

The selection of these two configurations made it possible to assess the additional contribution of building-envelope refurbishment under otherwise comparable PV-integrated conditions. For both scenarios, the electricity demand associated with space heating, cooling, dehumidification, and domestic hot-water production was derived from the corresponding retrofit configurations simulated in Termolog. Household appliances were initially excluded in order to distinguish system-related demand, which depends mainly on the technical characteristics of the retrofit solution, from occupant-dependent electricity use.

Scenario C represents the electricity demand associated with the main household appliances, namely the washing machine, dryer, dishwasher, refrigerator, television, and electric fan oven. The corresponding consumption profile was reconstructed using the nominal power of each appliance, the duration and frequency of use, and, where applicable, seasonal operating conditions. The resulting profile should therefore be interpreted as a representative use pattern for a three-person household rather than as a continuously monitored record of the occupants' electricity consumption. Actual consumption may vary depending on occupant behavior, appliance performance, and operating schedules.

Scenarios D and **E** were obtained by superimposing the appliance-demand profile defined in Scenario C on the system-related demand profiles of Scenarios A and B, respectively. They therefore represent the total household electricity demand under the two selected retrofit pathways. Since the same appliance profile and occupancy assumptions were applied in both cases, the differences between Scenarios D and E can be primarily attributed to the technical performance of the corresponding retrofit configurations. The composition and annual electricity demand of each scenario are summarized in Table 1.

Table 1: Definition and annual electricity demand of the selected retrofit scenarios.

Scenario	Reference Configuration and Included Loads	Scenario Definition	Annual Electricity Demand [kWh/year]
A	E2+F configuration	System-related electricity demand of the best-performing PV-integrated configuration without envelope refurbishment; household appliances excluded	4481.80
B	A+B+E1+F configuration	System-related electricity demand of the best-performing comprehensive PV-integrated retrofit configuration; household appliances excluded	3146.67
C	Main household appliances: washing machine, dryer, dishwasher, refrigerator, television, and electric fan oven	Appliance-use profile for a three-person household consisting of two adults and one teenager	574.15

(Continued)

Table 1 (continued)

Scenario	Reference Configuration and Included Loads	Scenario Definition	Annual Electricity Demand [kWh/year]
D	Scenario A + Scenario C	Total household electricity demand for the E2+F configuration, including system loads and household appliances	5055.96
E	Scenario B + Scenario C	Total household electricity demand for the A+B+E1+F configuration, including system loads and household appliances	3720.82

3 Definition of the Power Consumption Profiles for Each Scenario

Based on the electricity-demand scenarios defined in Section 2.2, monthly and daily electricity-consumption profiles for 2023 were reconstructed to compare the apartment's electricity use with the electricity generated by the 3 kWp PV system. For each scenario, the annual electricity demand was distributed over time according to the operating characteristics, seasonal behavior, and expected usage patterns of the corresponding systems and appliances. The specific assumptions and temporal-allocation criteria adopted for each scenario are described in the following subsections.

Heating-related electricity demand was assigned primarily to the winter months, whereas cooling-related demand was allocated to the summer months. Electricity demand for domestic hot-water production was distributed throughout the year, accounting for its expected seasonal variation. Household-appliance loads were allocated according to the assumed frequency and duration of use associated with the occupancy profile adopted for the case study.

The same temporal-allocation methodology was applied consistently across all scenarios to ensure comparability while accounting for the specific characteristics of each configuration. The resulting monthly electricity-consumption profiles for 2023 are presented in the following figures and provide the basis for comparison with PV electricity generation. The corresponding detailed daily electricity-consumption profiles for 2023 are reported in Appendix A.

3.1 Scenario A

Scenario A represents the system-related annual electricity demand associated with the E2+F configuration, which includes a 2 kW electric storage water heater for domestic hot-water production and a 5.1 kW air-to-air heat pump consisting of one outdoor unit and three indoor units for space heating, cooling, and dehumidification. Household-appliance loads were excluded from this scenario.

The total annual electricity demand was estimated at 4481.80 kWh. For the purpose of reconstructing the electricity-consumption profile, 20% of the annual demand, corresponding to 896.36 kWh/year, was attributed to domestic hot-water production, while the remaining 80%, corresponding to 3585.44 kWh/year, was assigned to the operation of the air-to-air heat pump. To account for seasonal variations in energy use, the annual demand was further divided between the winter period, from October to March, and the summer period, from April to September.

For domestic hot-water production, 63% of the annual electricity demand, equal to 564.71 kWh, was allocated to the winter period, while 37%, equal to 331.65 kWh, was assigned to the summer period, reflecting the assumed seasonal variation in hot-water demand.

For the air-to-air heat pump, 70% of its annual electricity demand, corresponding to 2509.81 kWh, was assigned to winter operation for space heating, whereas the remaining 30%, corresponding to 1075.63 kWh, was allocated to summer operation for cooling and dehumidification.

The monthly electricity-consumption profile was reconstructed by distributing the seasonal electricity demand among the corresponding months according to the assumed operating schedules of the systems. As shown in Fig. 5, electricity consumption is higher during the winter months because of space-heating requirements and decreases during the intermediate and summer periods, when the heat pump is used mainly for cooling and dehumidification.

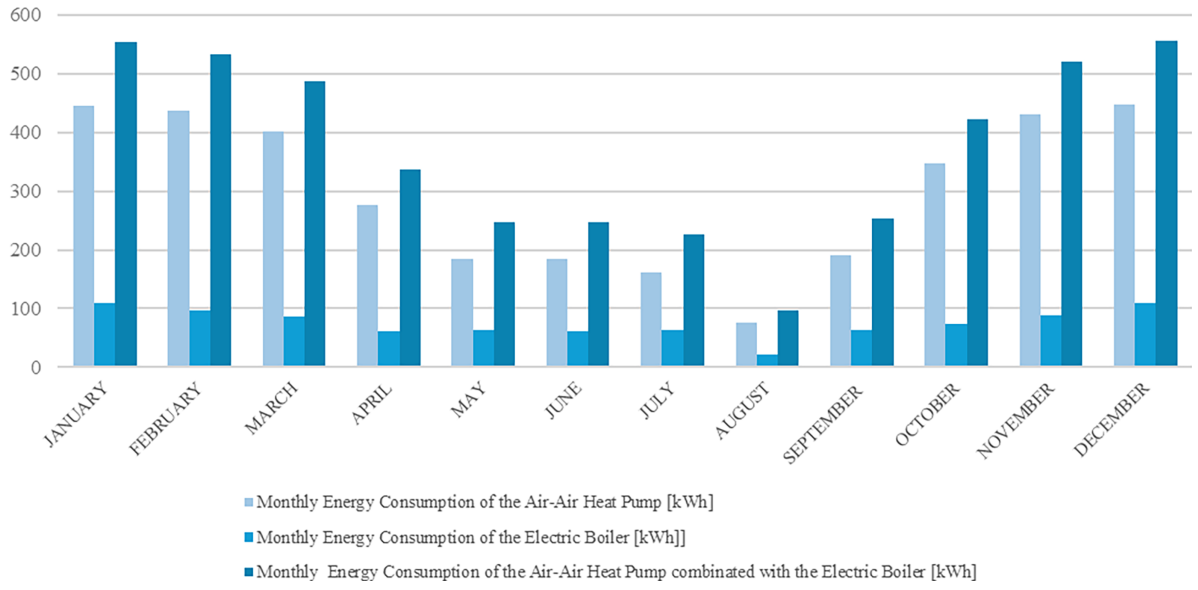


Figure 5: Monthly electricity-consumption profile for Scenario A in 2023, showing the individual contributions of the air-to-air heat pump and the electric water heater and their combined monthly demand.

The corresponding daily electricity-consumption profiles were subsequently derived from the monthly values by considering representative operating periods for the heat pump and the electric water heater. Finally, the profiles were normalized to ensure consistency with the annual electricity demand adopted for Scenario A. The detailed daily electricity-consumption profiles for the selected winter and summer months are reported in Appendix A.1.1.

3.2 Scenario B

Scenario B represents the system-related annual electricity demand associated with the A+B+E1+F configuration, which includes a 4.3 kW air-to-water heat pump for space heating and domestic hot-water production and a 5.1 kW air-to-air heat pump with one outdoor unit and three indoor units for cooling and dehumidification.

The air-to-water heat pump is coupled with a 166 L domestic hot-water storage tank and aluminum radiators. Household-appliance loads were excluded from this scenario. The total annual electricity demand was estimated at 3146.67 kWh. For the purpose of reconstructing the electricity-consumption profile, 70% of

the annual demand, corresponding to 2202.63 kWh/year, was assigned to the air-to-water heat pump, while the remaining 30%, corresponding to 944.01 kWh/year, was attributed to the air-to-air heat pump.

To account for seasonal variations in system operation, the annual electricity demand was further distributed between the winter period, from October to March, and the summer period, from April to September. For the air-to-water heat pump, 70% of its annual electricity demand, equal to 1541.87 kWh, was allocated to the winter period, when the system provides both space heating and domestic-hot-water production. The remaining 30%, equal to 660.80 kWh, was assigned to the summer period, primarily for domestic-hot-water production.

For the air-to-air heat pump, 10% of its annual electricity demand, corresponding to 94.40 kWh, was allocated to the winter period, whereas the remaining 90%, corresponding to 849.60 kWh, was assigned to summer operation for cooling and dehumidification.

The monthly electricity-consumption profile was reconstructed by distributing the seasonal electricity demand among the corresponding months according to the assumed operating schedules of the two heat-pump systems. As shown in Fig. 6, the air-to-water heat pump accounts for most of the electricity consumption during the heating season, whereas the contribution of the air-to-air heat pump increases during the summer months because of cooling and dehumidification requirements.

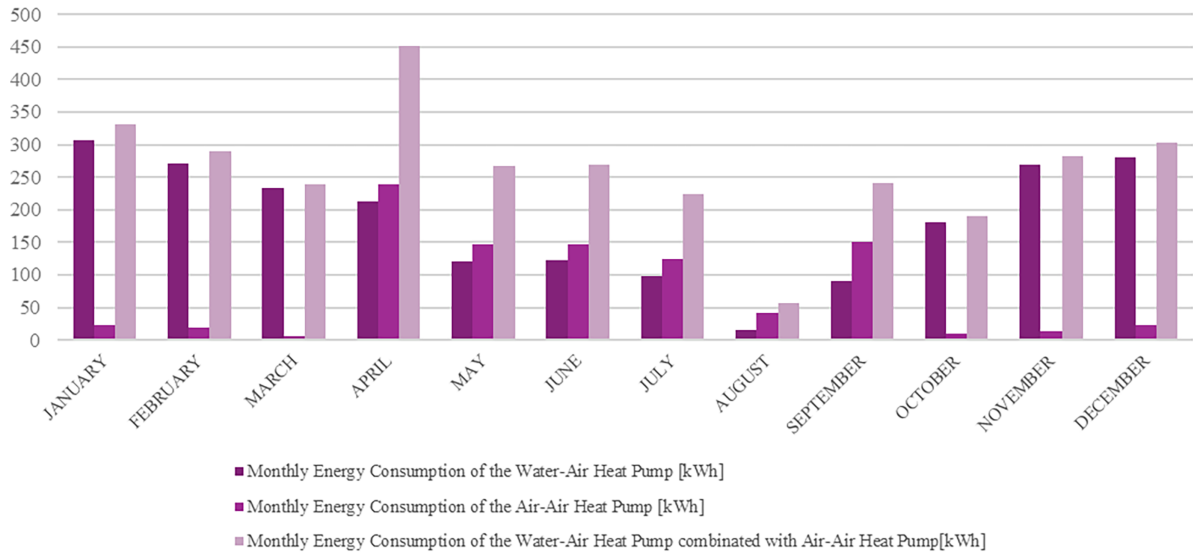


Figure 6: Monthly electricity-consumption profile for Scenario B in 2023, showing the individual contributions of the air-to-water and air-to-air heat pumps and their combined monthly consumption.

The corresponding daily electricity-consumption profiles were subsequently derived from the monthly values by considering representative operating periods for the two systems. Finally, the profiles were normalized to ensure consistency with the annual electricity demand adopted for Scenario B. The detailed daily electricity-consumption profiles for the selected winter and summer months are reported in Appendix A.1.2.

3.3 Scenario C

Scenario C represents the annual electricity demand associated exclusively with the main household appliances used by the occupants of the case-study apartment. To provide a realistic yet manageable representation of occupant-dependent electricity use, the analysis was limited to appliances that typically account for a substantial share of residential electricity consumption and exhibit recurring usage patterns.

The selected appliances were the washing machine, dryer, dishwasher, refrigerator, television, and electric fan oven. System-related loads associated with space heating, cooling, dehumidification, and domestic hot-water production were excluded from this scenario.

The annual electricity demand of each appliance was estimated by combining its technical specifications with representative usage patterns derived from the household-use questionnaire. The reference household consisted of two adults and one teenager. For appliances with a fixed electricity consumption per cycle, annual demand was calculated by multiplying the energy consumed per cycle by the assumed number of operating cycles. For appliances characterized by hourly electricity consumption, annual demand was calculated from the hourly consumption rate and the assumed operating time. Refrigerator demand was based directly on the manufacturer's declared annual electricity-consumption value. The assumptions adopted for each appliance are summarized in Table 2.

Table 2: Characteristics and operating assumptions of the household appliances considered in Scenario C.

Household Appliance	Energy Class	Electricity Consumption	Assumed Use Pattern
Washing machine	A	0.672 kWh/cycle	3 cycles/week; average cycle duration 1.5 h
Dryer	D	0.608 kWh/cycle	1 cycle/week during winter and rainy periods; average cycle duration 2 h
Dishwasher	A	0.301 kWh/cycle	1 cycle/day; average cycle duration 2 h
Refrigerator	A	108 kWh/year	Continuous operation throughout the year
Television	E	0.085 kWh/h	2.5 h/day on weekdays; 5 h/day on weekends
Electric fan oven	C	0.35 kWh/cycle	Variable use; operating time ranging from 10 min to 2.5 h depending on the cooking mode

Based on these assumptions, the annual electricity demand of each appliance was calculated. As shown in Fig. 7, the electric fan oven accounts for the largest share of annual electricity consumption, followed by the refrigerator, television, dishwasher, washing machine, and dryer.

The monthly electricity-consumption profile was subsequently reconstructed by distributing the annual electricity demand of each appliance according to its assumed frequency of use and seasonal operating pattern. Refrigerator consumption was distributed throughout the year as a nearly constant base load. Washing-machine and dishwasher loads were allocated throughout the year according to their assumed operating frequencies. Television consumption was distributed by distinguishing between weekdays and weekends. Dryer consumption was assigned primarily to the winter months and to periods characterized by limited opportunities for natural drying, whereas oven consumption was allocated according to the assumed cooking frequency.

Daily electricity-consumption profiles were then reconstructed by assigning each appliance load to representative operating periods derived from the questionnaire. Cycle-based appliances were modeled as

discrete operating events, whereas refrigerator consumption was distributed continuously throughout the day as a base load. The resulting profiles were normalized to ensure consistency with the monthly and annual electricity-demand values calculated for Scenario C.

The total annual electricity demand associated with Scenario C was estimated at 574.15 kWh/year. The resulting monthly electricity-consumption profile is presented in Fig. 8, while the detailed daily electricity-consumption profiles for the selected winter and summer periods are reported in Appendix A.1.3. The corresponding daily PV-demand balance and energy-management profiles are presented in Appendix A.2.1 as the appliance-only reference case.

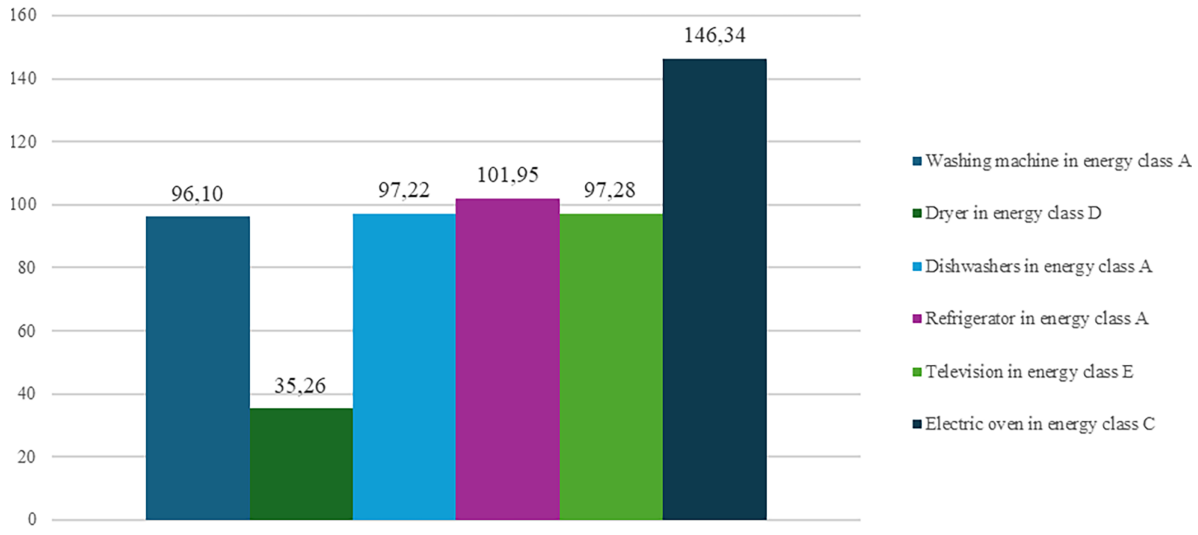


Figure 7: Annual electricity consumption of the main household appliances included in Scenario C (kWh/year).

3.4 Scenario D

Scenario D combines the system-related electricity demand of Scenario A with the household-appliance demand of Scenario C. It therefore represents the total household electricity demand associated with the E2+F configuration. The total annual electricity demand was estimated at 5055.96 kWh/year.

The monthly electricity-consumption profile was obtained by superimposing the system-related profile of Scenario A on the household-appliance profile of Scenario C.

As shown in Fig. 9, the resulting profile is driven primarily by system-related loads during the winter months, while the contribution of household appliances becomes more evident during periods of lower space-heating demand.

Separate daily electricity-consumption profiles are not reported for Scenario D because its demand is already represented within the daily PV-demand balance and energy-management profiles presented in Appendix A.2.2.

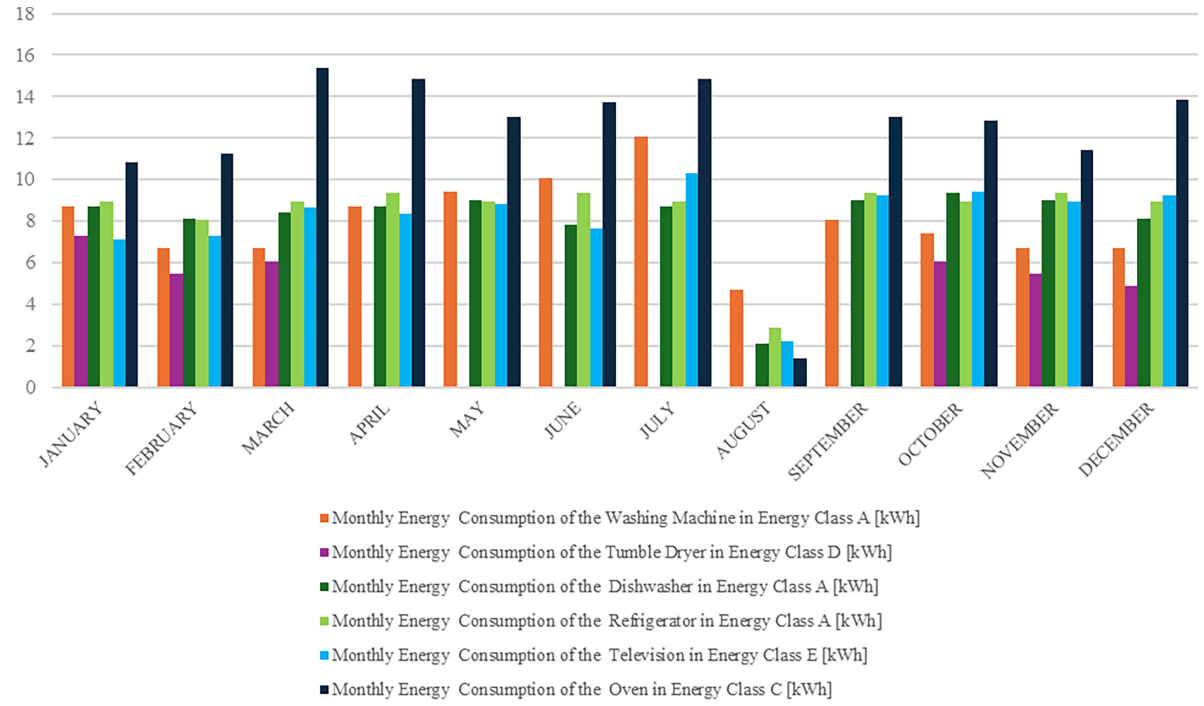


Figure 8: Monthly electricity-consumption profile for Scenario C in 2023.

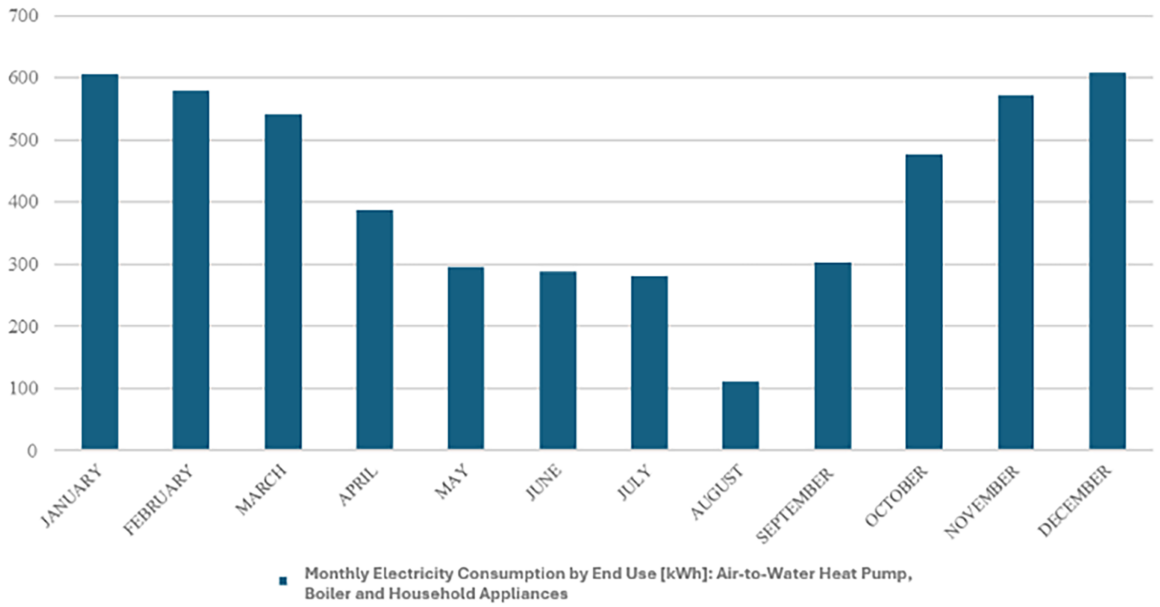


Figure 9: Monthly electricity-consumption profile for Scenario D in 2023, including the contributions of the air-to-air heat pump, electric water heater, and household appliances (kWh).

Scenario D has the highest annual electricity demand among the scenarios analyzed because it combines the substantial winter loads associated with the air-to-air heat pump and electric water heater with the year-round contribution of household appliances. The monthly electricity-consumption profile is driven primarily by system-related loads, particularly in January and December, whereas the contribution of household

appliances becomes more evident during months with lower space-heating demand. The minimum monthly consumption occurs in August, when both household activity and system operation are reduced. Scenario D therefore represents the most critical case for the PV energy-balance analysis because peak electricity demand occurs during the winter months, when PV generation is generally lower.

3.5 Scenario E

Scenario E was obtained by combining the system-related electricity demand of Scenario B with the household-appliance demand of Scenario C. It therefore represents the total household electricity demand associated with the A+B+E1+F retrofit configuration. The resulting annual electricity demand was estimated at 3720.82 kWh/year.

The monthly electricity-consumption profile was obtained by superimposing the system-related profile of Scenario B on the household-appliance profile of Scenario C. As shown in Fig. 10, the resulting profile includes the contributions of the air-to-water and air-to-air heat pumps, together with household-appliance consumption. Separate daily electricity-consumption profiles are not reported for Scenario E because its demand is already represented within the daily PV-demand balance and energy-management profiles presented in Appendix A.2.3.

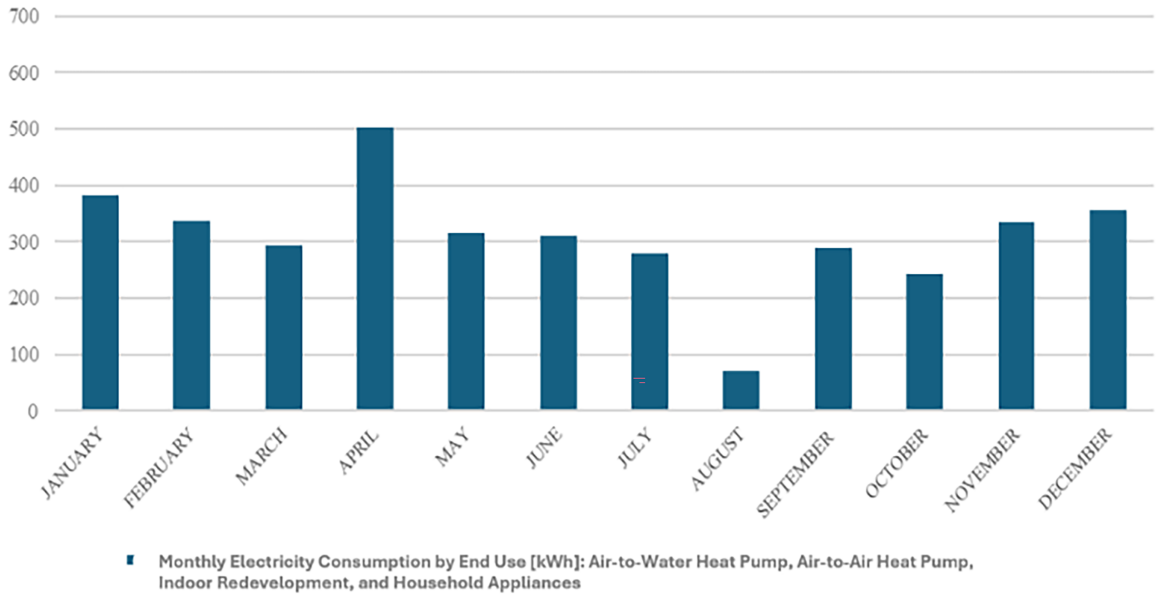


Figure 10: Monthly electricity-consumption profile for Scenario E in 2023, including the contributions of the air-to-water heat pump, air-to-air heat pump, and household appliances (kWh).

Scenario E represents the total electricity-consumption profile of the most energy-efficient combined retrofit configuration. Although the inclusion of household appliances increases the annual electricity demand relative to Scenario B, total consumption remains substantially lower than in Scenario D. This result confirms the effectiveness of the A+B+E1+F configuration, in which improved envelope performance and high-efficiency systems reduce the electricity required for space heating and cooling. The monthly profile still exhibits seasonal variation, although the winter peaks are less pronounced than those observed for Scenario D. Scenario E therefore represents the most favorable complete-load case for increasing PV self-consumption and reducing reliance on the electricity grid.

4 Methodology for Photovoltaic Production and Shading Assessment

The photovoltaic production profile was estimated through a two-step methodology combining a reference simulation with a site-specific shading assessment.

First, the Photovoltaic Geographical Information System (PVGIS), developed by the Joint Research Centre (JRC) of the European Commission, was used to estimate the photovoltaic energy production associated with the climatic conditions, geographical location, and technical configuration of the system [14].

Second, an analytical procedure was applied to account for the shading caused by surrounding obstacles, which are not explicitly represented in the standard PVGIS simulation. The analytical shading results were subsequently verified using a three-dimensional model developed in SketchUp Pro.

The photovoltaic array was assumed to be installed on the garage roof. This location was selected because the condominium roof did not provide a sufficiently large and unobstructed surface owing to the presence of dormers. In contrast, the garage roof provided an available installation area of approximately 16.53 m^2 and was therefore considered the most suitable location for accommodating the photovoltaic modules.

The proposed use of the garage roof was also considered compatible with the applicable regulatory conditions, in accordance with ruling no. 1337 of 17 January 2023, issued by the Lazio Regional Administrative Court.

The selected installation area and the proposed module arrangement are shown in Fig. 11.

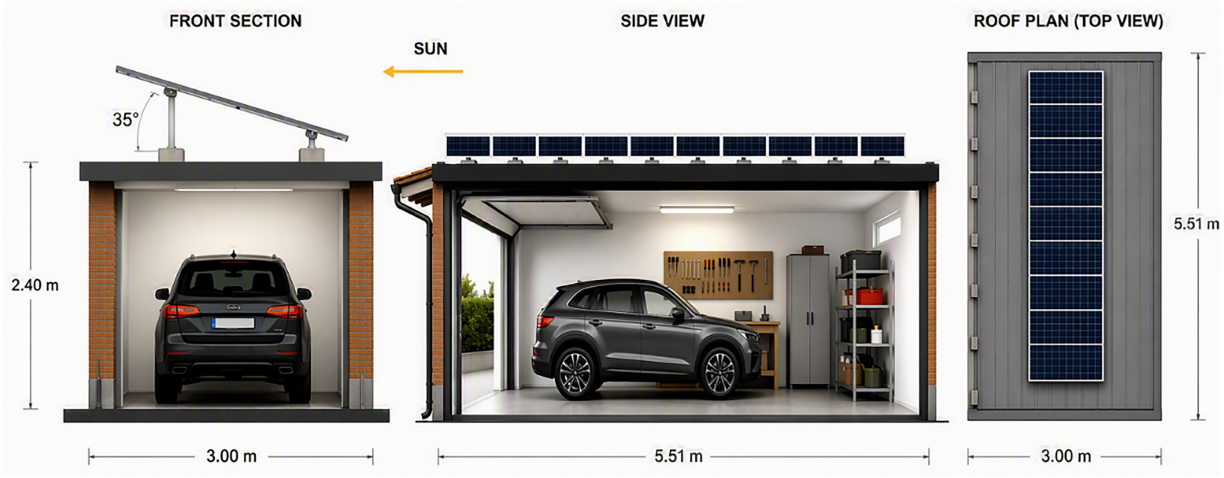


Figure 11: Proposed layout of the PV system on the garage roof, developed using Solar PV software.

The nominal capacity of the PV system was determined based on the available installation area and the dimensions and rated power of the selected modules. As a preliminary sizing criterion, the maximum installable photovoltaic capacity was calculated using Eq. (1) [15]:

$$P_{max} = k\frac{S_u}{S_m} \tag{1}$$

where P_{max} is the maximum installable photovoltaic capacity (kWp), K_{arr} is a coefficient accounting for the module arrangement, A_u is the available installation area (m^2), and k is the specific surface coefficient of the selected photovoltaic technology (m^2/kWp). A value of 1 was assigned to K_{arr} because the modules were installed without spacing between adjacent rows. Based on the available area of 16.53 m^2, Eq. (1) yielded a maximum installable capacity of approximately 3 kWp.

The number of photovoltaic modules was then determined using Eq. (2) [15]:

$$n^{\circ}_{PV_{panels}} = \frac{S_u}{S_p} \tag{2}$$

where N_{PV} is the number of photovoltaic modules, A_u is the available installation area, and A_{mod} is the area of a single module (m^2). The selected modules measured 1.65 m × 0.99 m, corresponding to an area of approximately 1.63 m^2 per module. Based on the available installation area, ten modules could be installed. Since each module had a rated power of 300 W, the resulting nominal system capacity was 3 kWp.

The nominal photovoltaic conversion efficiency was also evaluated from the relationship between the installed peak power, the total active module area, and the standard irradiance of 1 kW/m^2, as expressed by Eq. (3) [15–17]:

$$e_{\%} = \frac{P_{max}}{\frac{S_u}{1000}} \tag{3}$$

where η_{PV} is the photovoltaic conversion efficiency, P_{max} is the nominal peak power, and A_{PV} is the total active module area. Application of Eq. (3) yielded an efficiency of approximately 18.75%. This value is in close agreement with the module efficiency of 18.98% reported in the manufacturer's technical specifications. The manufacturer's value was therefore adopted for the subsequent photovoltaic production calculations, while the calculated value was used as an independent consistency check.

The parameters listed in Table 3 define the technical configuration, methodological assumptions, and scope of the photovoltaic production and shading assessment.

Table 3: Main geometrical, technical, and environmental parameters considered in the photovoltaic production model.

Parameter	Adopted Value	Source or Justification
LATITUDE	45.43° N	Installation-site coordinates
LONGITUDE	9.32° E	Installation-site coordinates
AVAILABLE INSTALLATION AREA	16.53 m^2	Geometric assessment of the garage roof
NUMBER OF MODULES	10	Derived from the available area and module dimensions
MODULE DIMENSIONS	1.65 m × 0.99 m	Manufacturer's technical data
SINGLE-MODULE AREA	1.63 m^2	Manufacturer's technical data
RATED POWER PER MODULE	300 W	Manufacturer's technical data
NOMINAL SYSTEM CAPACITY	3 kWp	Ten 300 W modules
MODULE EFFICIENCY	18.98%	Manufacturer's technical data
CALCULATED EFFICIENCY	18.75%	Consistency check using Eq. (3)
TEMPERATURE COEFFICIENT	−0.389%/°C	Manufacturer's technical data
ASSUMED MODULE OPERATING TEMPERATURE	42°C	Technical documentation supplied by the photovoltaic system provider

(Continued)

Table 3 (continued)

Parameter	Adopted Value	Source or Justification
TILT ANGLE	35°	Technically reasonable value for site latitude and compatible with installation geometry; not separately optimized
AZIMUTH ANGLE	180°	South-facing configuration, using the PVGIS azimuth convention
HORIZONTAL OBSTACLE DISTANCE	50 m	Site geometrical assessment
RELATIVE OBSTACLE HEIGHT	12.8 m	Measured vertical height difference between the top of the obstacle and the base reference level of the photovoltaic array.
EFFECTIVE OBSTACLE HEIGHT	10.91 m	Height difference between the obstacle top and the upper edge of the 35°-tilted photovoltaic array

The energy system considered in the subsequent energy-balance and self-consumption analysis consisted of a grid-connected hybrid photovoltaic system comprising the 3 kWp photovoltaic array described in this section and a 5 kWh battery storage unit. In this configuration, photovoltaic generation can directly supply household electricity demand, excess electricity can be stored in the battery for later use, and any remaining demand is met by the utility grid [4,5,7]. The battery was not included in the photovoltaic production calculations presented in this section because energy storage does not affect the amount of electricity generated by the photovoltaic modules. Its operation was evaluated only in the subsequent analysis of electricity production and demand, where its effects on self-consumption, energy storage, battery utilization, and grid exchanges were assessed.

For the photovoltaic production assessment, the array was modeled as ten identical modules rated at 300 W each, corresponding to a total installed capacity of 3 kWp. The modules were assumed to be installed at a fixed tilt angle of 35° and a south-facing azimuth of 180°. This tilt angle was selected as a technically reasonable value for the site latitude and as compatible with the available garage-roof geometry; it was not derived through a separate optimization process. Module dimensions, rated power, nominal conversion efficiency (18.98%), and temperature coefficient (−0.389%/°C) were obtained from the manufacturer's specifications. A constant operating temperature of 42°C, taken from the documentation provided by the photovoltaic system supplier, was assumed throughout the analysis. Consequently, hourly and seasonal temperature variations were not explicitly modeled.

PVGIS was used solely to generate a standardized reference production profile based on site location, climatic conditions, installed capacity, module tilt, and orientation. The influence of surrounding obstacles was evaluated independently through a site-specific geometric shading model incorporating measured obstacle dimensions and distances, array geometry, and solar position for each analyzed time step. A shading event was considered to occur only when the shadow cast by an obstacle both reached the photovoltaic array and intersected the plan-view footprint of the modules. The resulting sunlit fraction of the array was then used in the analytical production calculations.

Because detailed information regarding module interconnections, string configuration, bypass-diode behavior, inverter maximum-power-point tracking, and electrical mismatch losses was unavailable, photovoltaic output was assumed to vary linearly with the fraction of module area directly exposed to sunlight.

This simplification allowed the geometric effects of partial shading to be represented while acknowledging that the nonlinear electrical losses associated with nonuniform irradiance were not explicitly modeled.

The analytical irradiation approach was therefore intended as a simplified screening-level direct-beam model. Atmospheric attenuation, cloud-cover effects, diffuse irradiation, and ground-reflected irradiation were not modeled separately. Consequently, the analytical results and the PVGIS estimates were treated as complementary rather than sequential outputs. Their comparison was used to evaluate the plausibility of seasonal production trends and to assess the influence of the site-specific geometric, temperature, and shading assumptions. The comparison was not intended to reproduce PVGIS results exactly, quantify shading losses through direct subtraction, or provide a bankable energy-yield prediction.

4.1 Reference Photovoltaic Production Estimated Using PVGIS

PVGIS was used to determine a reference photovoltaic production profile based on the climatic conditions of the installation site.

The simulation was performed using the geographical coordinates of 45.43° N and 9.32° E, a nominal system capacity of 3 kWp, a south-facing orientation corresponding to an azimuth angle of 180°, and a module tilt angle of 35°.

This inclination was considered suitable for maximizing annual photovoltaic energy production at the site latitude while remaining compatible with the geometric constraints of the installation area [6,15,16].

The PVGIS simulation provided monthly photovoltaic energy production and the corresponding solar irradiation on the plane of the photovoltaic modules for the year 2023.

These results were used as the reference case prior to applying the site-specific correction for local shading conditions.

As shown in Fig. 12, the reference production profile exhibits the expected seasonal variation, with higher values during the summer months and lower values during winter. The highest monthly production was recorded in July, reaching 503.21 kWh and corresponding to a solar irradiation of 221.23 kWh/m^2. The lowest monthly production occurred in December, with a value of 157.05 kWh and a corresponding solar irradiation of 68.77 kWh/m^2. On an annual basis, PVGIS estimated a total photovoltaic energy production of 4022.01 kWh and a total solar irradiation on the module plane of 1765.92 kWh/m^2. These values were adopted as the uncorrected reference case for the subsequent shading assessment.

4.2 Site-Specific Shading Assessment

A site-specific shading assessment was performed to account for the effects of the surrounding building geometry on the photovoltaic array. Although PVGIS provides a reference production profile based on the site climate and technical configuration, the standard simulation adopted in this study does not explicitly reproduce the detailed three-dimensional geometry of nearby obstacles. An additional analytical procedure was therefore introduced to determine, for each analyzed date and local time, whether the shadow cast by the surrounding building reached the photovoltaic modules and to estimate the resulting reduction in direct solar exposure [6,15,18,19].

The shading analysis was based on the geometric relationship among the photovoltaic array, the surrounding obstacle, and the position of the sun. The relative obstacle height was defined as the vertical difference between the top of the obstacle and the base reference level of the photovoltaic array. This height was calculated as 15.0 − 2.2 = 12.8 m. Because the photovoltaic array was inclined by 35° and had a dimension of 3.30 m along the inclined direction, its upper edge was 3.30 sin(35°) = 1.89 m above the base

reference level. Accordingly, the effective vertical obstacle height used in the shadow-length calculation was 12.8 − 1.89 = 10.91 m. The horizontal distance between the obstacle and the photovoltaic array was 50 m.

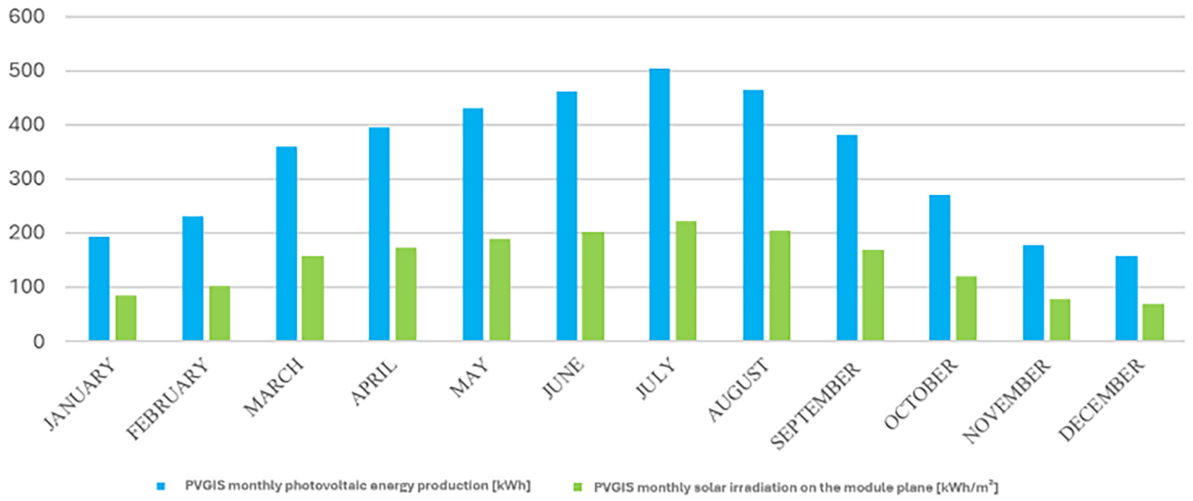


Figure 12: Monthly photovoltaic energy production and solar irradiation incident on the module plane, as estimated using PVGIS for the year 2023.

The procedure consisted of three consecutive steps. First, the solar elevation and azimuth angles were determined from the geographical coordinates, selected date, and local time. Second, the solar elevation angle was used to calculate the horizontal shadow length. Third, the calculated length and shadow direction were jointly compared with the obstacle-to-array distance and the planimetric position of the photovoltaic array. A shading event was considered to occur only when the shadow both reached the array and was directed toward its footprint. The resulting unshaded fraction was then used in the photovoltaic production calculation.

4.2.1 Solar Position

The solar position was determined using the SunEarthTools application based on the geographical coordinates of the installation site, the selected date, and the local time [19]. The coordinates used in the analysis were 45.43° N latitude and 9.32° E longitude, consistent with those adopted in the PVGIS simulation.

For each analyzed time step, SunEarthTools provided both the solar elevation angle (θ) and the solar azimuth angle. The analyzed time steps corresponded to the dates and local times used in the calculation dataset and were subsequently aggregated to obtain monthly results. The solar elevation angle represents the angular height of the sun above the horizon and directly affects the length of the shadow cast by the surrounding obstacle. Lower solar elevation angles result in longer shadows, whereas higher solar elevation angles produce shorter shadows [18,19].

The solar azimuth angle, obtained from the same SunEarthTools output, was used to determine the horizontal direction of the sun and therefore the direction of the resulting shadow relative to the photovoltaic array. This verification was necessary because shadow length alone does not establish whether the shadow intersects the modules. Only the combined analysis of solar elevation, solar azimuth, obstacle position, and array footprint made it possible to identify an effective shading condition.

The annual solar elevation profile for the installation site is shown in Fig. 13. The profile illustrates both daily and seasonal variations in solar elevation, with lower values occurring during winter and in the early morning and late afternoon, and higher values occurring around solar noon and during the summer months.

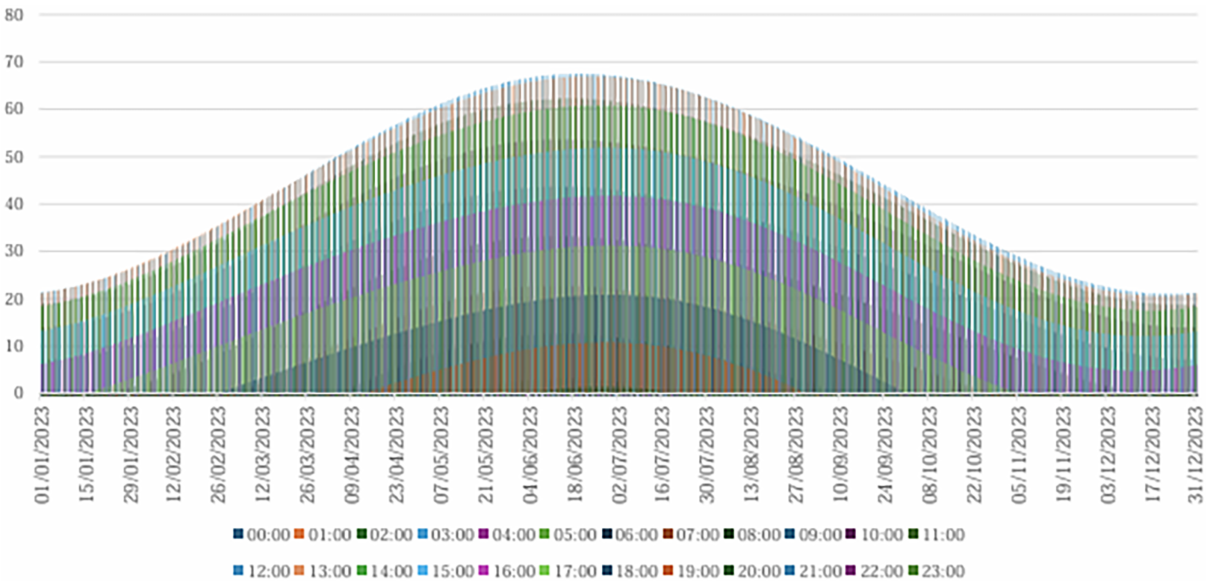


Figure 13: Annual solar elevation profile generated with SunEarthTools based on the geographic coordinates of the installation site.

As shown in Fig. 13, the lowest solar elevation angles occur during winter and near sunrise and sunset, producing the longest potential shadows. Conversely, the higher solar elevation angles observed in summer result in shorter shadow lengths.

4.2.2 Shadow-Length Calculation

The shadow length produced by the surrounding obstacle was calculated based on the geometric relationship between the relative obstacle height and the solar elevation angle [18,19].

$$L = \frac{h}{\tan(\theta)} \tag{4}$$

where L is the horizontal shadow length (m), h is the effective vertical height difference between the top of the obstacle and the upper edge of the photovoltaic array (m), and θ is the solar elevation angle (°).

In this study, an effective vertical obstacle height of 10.91 m was adopted. The relative obstacle height measured from the base reference level of the photovoltaic array was 12.8 m. The vertical rise of the 3.30 m-long photovoltaic array inclined at 35° was calculated as 3.30 sin(35°) = 1.89 m. Therefore, the effective height difference between the top of the obstacle and the upper edge of the photovoltaic array was calculated as 12.8 − 1.89 = 10.91 m. The 35° module tilt was used only to determine the elevation of the upper edge of the photovoltaic array; the solar elevation angle obtained from SunEarthTools was used in Eq. (4) to calculate the horizontal shadow length at each time step.

4.2.3 Shaded Fraction of the Photovoltaic Array

The calculated shadow length was compared with the horizontal distance between the obstacle and the photovoltaic array. If the shadow length was shorter than the obstacle-to-array distance, the array was considered fully exposed to direct sunlight. If the shadow reached the array, the solar azimuth was additionally checked to verify that the shadow direction intersected the array footprint. Only after both

conditions were satisfied was the shaded portion evaluated relative to the array dimension along the shadow direction.

The shaded fraction of the photovoltaic array was calculated using Eq. (5):

$$f_{sh} = max\left[0, min\left(1, \frac{L-d}{l_{PV}}\right)\right] \tag{5}$$

where f_{sh} is the shaded fraction of the photovoltaic array; L is the calculated shadow length; d is the horizontal distance between the obstacle and the photovoltaic array, equal to 50 m; and l_{PV} is the dimension of the photovoltaic array measured in the direction of the shadow. All length parameters are expressed in meters.

The corresponding fraction of the array exposed to direct sunlight was then calculated according to Eq. (6):

$$f_{sun} = 1 - f_{sh} \tag{6}$$

where f_{sun} ranges from 0 to 1. A value of 1 indicates full exposure of the array to direct sunlight, whereas a value of 0 indicates complete shading.

4.3 Independent Analytical Calculation of Photovoltaic Production

The photovoltaic production values reported as "calculated" were obtained from an analytical, screening-level procedure independent of the monthly PVGIS results. PVGIS was retained as a standardized external reference, whereas the analytical model was developed to make the site-specific geometry and shading assumptions explicit. The PVGIS irradiation values were therefore neither used as direct inputs to the analytical energy calculation nor multiplied by a shading factor. At each analyzed time step, SunEarthTools supplied the solar elevation and azimuth for the site coordinates, date, and local time. Solar elevation was used to estimate a simplified direct-beam irradiance component, while obstacle geometry and solar azimuth were used to determine whether the resulting shadow reached and intersected the photovoltaic array. The directly illuminated fraction, $f_{sun,t}$, was then calculated as described in Section 4.2.3.

The effective direct solar irradiance at each time step was calculated using the simplified relationship presented in Eq. (7):

$$I_t = I_{sc} \cdot sin\left(\theta_t\right) \cdot f_{sun,t} \tag{7}$$

where I_t is the effective direct solar irradiance at time step t (W/m^2), I_{sc} is the adopted solar constant (1367 W/m^2), θ_t is the solar elevation angle, and $f_{sun,t}$ is the fraction of the photovoltaic array directly exposed to sunlight. The direct solar irradiance was estimated using a simplified approach based on the solar constant and solar elevation angle. Atmospheric attenuation, cloud cover effects, and the diffuse and ground-reflected components of solar radiation were not modeled separately.

The corresponding solar irradiation was obtained by integrating the calculated irradiance over the considered time interval:

$$G_t = \int I_t \, dt \tag{8}$$

where G_t is the calculated solar irradiation for the considered time interval (Wh/m^2). The time-step values were subsequently aggregated to obtain the monthly and annual irradiation profiles reported in Fig. 14 and Table 4.

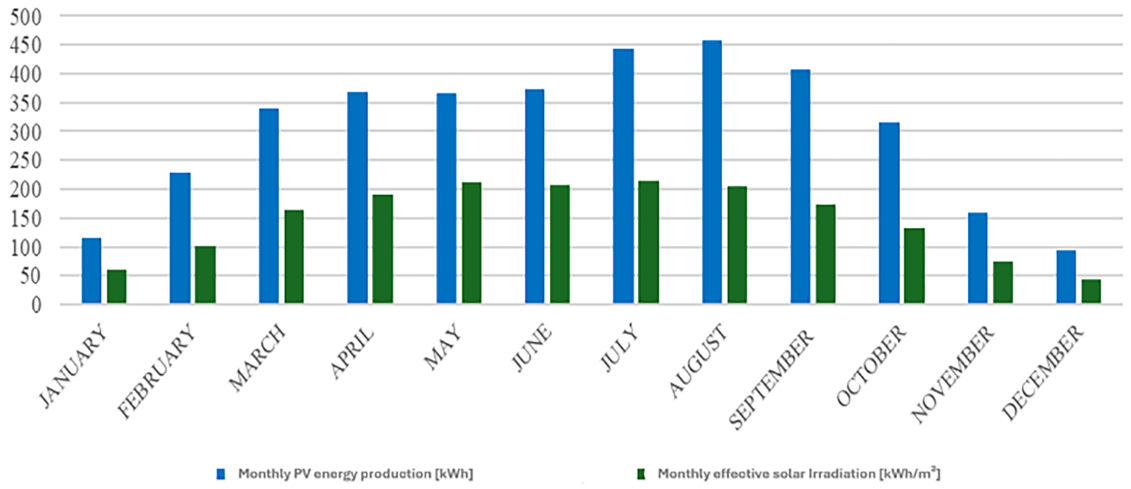


Figure 14: Monthly shading-corrected photovoltaic energy production and effective solar irradiation in 2023.

Table 4: Monthly comparison of photovoltaic energy production and solar irradiation obtained from the shading-corrected model and PVGIS for the year 2023.

Month	Monthly PV System Energy Production (Calculated) [kWh]	Monthly PV System Energy Production (PVGIS) [kWh]	Monthly Global Solar Irradiance (Calculated) [kWh/m^2]	Monthly Global Solar Irradiance (PVGIS) [kWh/m^2]
JANUARY	116.23	192.86	61.33	84.3
FEBRUARY	229.99	230.96	101.54	101.18
MARCH	340.07	359.64	163.75	157.65
APRIL	369.56	394.06	190.63	173.15
MAY	366.34	430.69	210.96	189.58
JUNE	372.72	460.57	206.27	202.74
JULY	443.71	503.21	214.14	221.23
AUGUST	457.41	462.89	204.07	203.38
SEPTEMBER	406.45	381.79	173.88	167.5
OCTOBER	315.45	271.58	133.07	119.03
NOVEMBER	160.28	176.71	74.08	77.41
DECEMBER	93.16	157.05	43.80	68.77
TOTAL	**3671.38**	**4022.01**	**1777.52**	**1765.92**

The photovoltaic energy production at each time step was then calculated using Eq. (9):

$$E_{PV,t} = G_{eff,t} A_{PV} \eta_{mod} f_T \tag{9}$$

where $E_{PV,t}$ denotes the photovoltaic energy generated at time step t (kWh), $G_{eff,t}$ denotes the effective irradiance received by the photovoltaic array (kWh/m^2), A_{PV} is the total active photovoltaic module area (m^2), η_{mod} is the nominal module efficiency (18.98%), and f_T is the temperature correction factor.

The temperature correction factor f_T was calculated according to Eq. (10):

$$f_T = 1 + \gamma(T_{mod} - T_{ref}) \tag{10}$$

where γ denotes the module temperature coefficient ($-0.00389°C^{-1}$), T_{mod} is the assumed operating temperature of the module (42°C), and T_{ref} is the standard reference temperature (25°C). Based on these assumptions, the calculated temperature correction factor is approximately 0.934, resulting in an estimated 6.6% reduction in nominal conversion efficiency.

The model assumes a linear relationship between the fraction of module area exposed to direct sunlight and photovoltaic output. This assumption was adopted because detailed information on module interconnections, string layout, inverter maximum-power-point tracking, and bypass-diode operation was not available. Consequently, the procedure represents the geometrical influence of shading but does not explicitly simulate electrical mismatch or other nonlinear losses caused by partial shading.

The analytical calculation and PVGIS are therefore complementary rather than sequential. The analytical model provides a transparent, site-specific assessment of obstacle geometry and direct-sun exposure, whereas PVGIS provides a standardized estimate based on local climatic databases and conventional system-loss assumptions. Because the two approaches use different irradiation models, atmospheric assumptions, temporal aggregation procedures, and loss treatments, the calculated monthly irradiation and production values may be either higher or lower than the corresponding PVGIS values. Their comparison should therefore be interpreted as a consistency assessment and not as a direct subtraction of shading losses from the PVGIS output.

Following the analytical irradiation, shading, and temperature calculations, the monthly photovoltaic production and corresponding calculated solar irradiation were obtained, as shown in Fig. 14.

The analytical model resulted in an annual photovoltaic energy production of 3671.38 kWh and an annual calculated solar irradiation of 1777.52 kWh/m^2. The monthly profile exhibits the expected seasonal variation, with lower values during winter and higher values during summer. The highest photovoltaic output was recorded in August, whereas the lowest occurred in December. A detailed comparison with the independent PVGIS reference is provided in Section 4.5.

4.4 Verification of the Shading Calculation

The analytical shading calculations were verified using a three-dimensional model developed in SketchUp Pro. The model reproduced the measured geometric relationship among the photovoltaic array, garage roof, and surrounding obstacle, allowing the calculated shadow direction and length to be compared with a graphical simulation. This verification was intended to check the internal geometric consistency of the analytical procedure rather than to provide an independent annual energy-yield prediction.

The summer solstice (21 June 2023) was selected as a transparent verification case because it combines high solar elevation with extended daylight duration and therefore clearly illustrates the daily change in shadow geometry. Three representative times were analyzed: 9:00 a.m., solar noon, and 4:00 p.m. These simulations were used only as graphical verification points and were not used as the sole basis for determining the annual shading correction.

At 9:00 a.m., the solar elevation angle was 43.43°, corresponding to a calculated horizontal shadow length of 11.52 m. At solar noon, the solar elevation angle increased to 67.45°, reducing the shadow length to 4.53 m. At 4:00 p.m., the solar elevation angle decreased to 41.53°, with a corresponding shadow length of 12.32 m. The SketchUp Pro simulations showed shadow geometries consistent with the analytical calculations, thereby providing a visual validation of the adopted shading model, as shown in Fig. 15a–c.

The three-dimensional model reproduced the expected daily variation in shadow length and showed close agreement with the analytical calculations. Accordingly, SketchUp served as a visual verification tool for selected geometric conditions, rather than as a substitute for the annual analytical assessment.

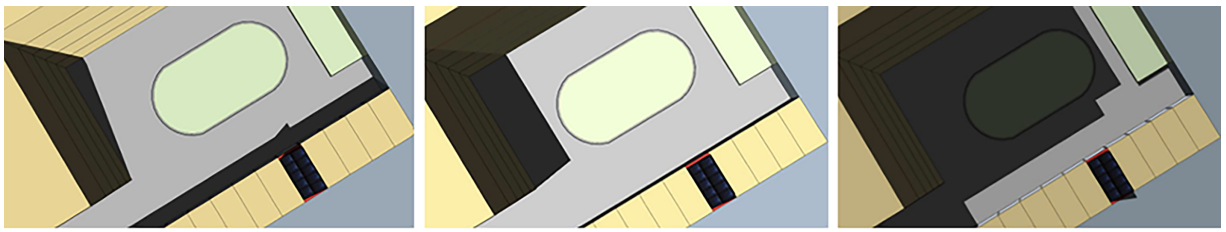


Figure 15: Three-dimensional verification of the shadow geometry using SketchUp Pro on 21 June 2023: (**a**) 9:00, solar elevation angle of 43.43° and calculated horizontal shadow length of 11.52 m; (**b**) solar noon, solar elevation angle of 67.45° and calculated horizontal shadow length of 4.53 m; (**c**) 16:00, solar elevation angle of 41.53° and calculated horizontal shadow length of 12.32 m.

4.5 Comparison of the Shading-Corrected Results with PVGIS

The monthly photovoltaic energy production and solar irradiation obtained from the independent analytical model were compared with the corresponding PVGIS reference values. The objective was not to demonstrate numerical identity or to interpret the analytical values as a direct correction of the PVGIS output. Instead, the comparison was used to evaluate the consistency of the seasonal trend and to discuss the influence of the site-specific geometrical, temperature, and shading assumptions. The results are summarized in Table 4.

The shading-corrected calculation resulted in an annual photovoltaic energy production of 3671.38 kWh, compared with 4022.01 kWh estimated by PVGIS. The difference between the two values was 350.63 kWh, corresponding to approximately 8.7% of the PVGIS reference value.

The most significant reductions were observed in January and December, when lower solar elevation angles increased the likelihood of interaction between the shadow cast by the surrounding obstacle and the photovoltaic array. During the summer months, the results obtained using the two approaches were generally more consistent, as the higher solar elevation angles reduced the obstacle's influence on the modules.

However, the estimated energy production obtained through the analytical calculation was higher than the value provided by PVGIS during the months of September and October. Similarly, the annual irradiation calculated using the analytical method amounted to 1777.52 kWh/m^2, a value slightly higher than the 1765.92 kWh/m^2 estimated by PVGIS.

These differences indicate that the comparison between the two approaches cannot be interpreted simply as the subtraction of shading losses from the PVGIS results. They also arise from the different calculation methodologies and assumptions adopted regarding incident solar irradiation, module operating temperature, conversion efficiency, temporal data aggregation, and overall system losses. Consequently, the monthly values obtained from the analytical model may be either higher or lower than the corresponding reference values provided by PVGIS, even when the total annual energy production remains lower.

In this study, PVGIS was used as a standardized reference based on the climatic conditions of the installation site and on conventional assumptions regarding the operation of the photovoltaic system. In contrast, the analytical approach incorporated a simplified representation of the geometry of surrounding obstacles and their impact on solar exposure.

A graphical comparison of the monthly results obtained using the two methods is presented in Fig. 16a,b.

Both approaches reproduced the expected seasonal variation in photovoltaic performance. PVGIS provided a standardized reference profile based on local climatic data and conventional system assumptions, while the analytical approach made the local geometric and shading assumptions explicit. The comparison

therefore improves the transparency of the assessment, but the analytical results should be interpreted within the stated simplifications concerning module temperature, irradiation components, and the linear treatment of partial shading.

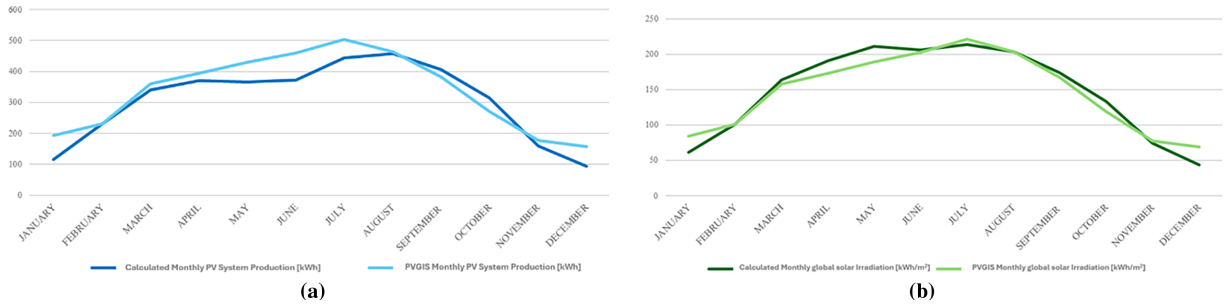


Figure 16: Comparison between the shading-corrected calculation and PVGIS for the year 2023: (**a**) Monthly photovoltaic energy production [kWh]; (**b**) Monthly global solar irradiation [kWh/m^2].

Accordingly, the results refer to the 2023 case-study conditions and should not be interpreted as an experimental validation or as a prediction of long-term average photovoltaic performance.

5 PV System Energy Balance and Residential Electricity Demand

To assess the contribution of battery energy storage to the overall performance of the photovoltaic system, a preliminary comparison was conducted between a conventional PV configuration without storage and a hybrid PV configuration equipped with a 5 kWh battery.

The analysis presented in this section focuses primarily on the hybrid configuration, whereas the system without storage serves as a reference case for the annual performance assessment.

In the hybrid configuration, PV generation first supplies the instantaneous household electricity demand. When generation exceeds demand, the surplus electricity is used to charge the battery up to its available capacity, after which any remaining energy is exported to the grid. Conversely, when household demand exceeds PV generation, available battery energy is discharged to meet the residual demand before electricity is imported from the grid.

This operating strategy reduces the temporal mismatch between PV generation and electricity consumption, thereby increasing the on-site utilization of locally generated electricity and reducing grid dependence [4,5,7,20]. The relationship between PV generation and household electricity demand was evaluated for the five electricity-demand scenarios defined in Section 3.

5.1 Monthly PV Generation–Demand Balance

To provide a comparative assessment of the relationship between PV generation and household electricity demand, the monthly net energy balance for the year 2023 was evaluated for Scenarios A–E.

For each month and scenario, the balance was calculated as the difference between PV generation estimated using the analytical method and the corresponding electricity demand according to Eq. (11):

$$E_{bal,m,s} = E_{PV,m} - E_{load,m,s} \tag{11}$$

where $\boldsymbol{E_{bal,m,s}}$ is the monthly net energy balance for month $\boldsymbol{m}$ and Scenario $\boldsymbol{s}$, $\boldsymbol{E_{PV,m}}$ is the monthly PV generation, and $\boldsymbol{E_{load,m,s}}$ is the corresponding monthly electricity demand. Positive values indicate that PV generation exceeds electricity demand, whereas negative values indicate an energy deficit.

Because the same PV system is considered in all scenarios, the generation profile remains unchanged, while electricity demand varies according to the retrofit configuration and the household loads included in each scenario. The resulting monthly balances are summarized in Table 5.

Table 5: Consolidated monthly net energy balance for Scenarios A–E in 2023, calculated as photovoltaic production estimated by the calculation method minus electricity demand.

Month	PV Calculation Method [kWh]	PVGIS Platform [kWh]	Net Energy Balance of Scenario A [kWh]	Net Energy Balance of Scenario B [kWh]	Net Energy Balance of Scenario C [kWh]	Net Energy Balance of Scenario D [kWh]	Net Energy Balance of Scenario E [kWh]
JANUARY	116.23	192.86	−438.2	−214.4	+64.6	−489.9	−266.1
FEBRUARY	229.99	230.96	−302.9	−59.7	+183.0	−349.9	−106.7
MARCH	340.07	359.64	−147.3	+101.6	+285.9	−201.5	+47.4
APRIL	369.56	394.06	+32.2	−82.8	+319.6	−17.7	−132.8
MAY	366.34	430.69	+119.6	+99.0	+317.1	+70.3	+49.8
JUNE	372.72	460.57	+125.6	+103.0	+324.1	+76.9	+54.3
JULY	443.71	503.21	+218.3	+219.7	+388.8	+163.4	+164.9
AUGUST	457.41	462.89	+360.5	+401.2	+444.1	+347.2	+387.9
SEPTEMBER	406.45	381.79	+152.8	+165.7	+357.7	+104.0	+116.9
OCTOBER	315.45	271.58	−107.7	+125.1	+261.5	−161.7	+71.1
NOVEMBER	160.28	176.71	−359.5	−123.0	+109.3	−410.5	−174.0
DECEMBER	93.16	157.05	−463.7	−210.6	+41.5	−515.4	−262.2
TOTAL	**3671.38**	**4022.01**	**−810.4**	**+524.7**	**+3097.2**	**−1384.6**	**−49.4**

Note: Green indicates a positive net energy balance (PV surplus), red indicates a negative net energy balance (energy deficit), and yellow indicates the annual totals.

At the annual scale, the comparison between electricity demand and photovoltaic generation provides a clear indication of the ability of the PV system to meet the energy requirements of each scenario.

As shown in Fig. 17, the bars represent the annual electricity demand, while the horizontal lines indicate the annual photovoltaic generation estimated using both the PVGIS model and the calculation-based method. Scenario C represents the most favorable condition, since the electricity demand associated with household appliances remains consistently below the available photovoltaic generation throughout the year.

Scenario B also achieves a positive annual energy balance, although support from the electricity grid is still required during the winter months, when photovoltaic generation decreases and electricity demand related to thermal systems increases. In contrast, Scenarios A and D represent the most critical configurations, as their annual electricity demand exceeds photovoltaic generation and significant energy deficits occur during the winter period. Scenario E represents an intermediate optimized configuration: its annual demand is close to the photovoltaic generation estimated by PVGIS, while the calculation-based method indicates a slight annual deficit due to the inclusion of site-specific factors, particularly shading effects.

A monthly assessment is therefore required to better understand how this annual performance is distributed throughout the year.

As shown in Fig. 18, the seasonal mismatch between photovoltaic generation and electricity demand is particularly evident during the winter months, when lower solar availability coincides with higher electricity demand, especially in Scenarios A and D.

In contrast, spring and summer exhibit a more favorable energy balance, with surplus conditions occurring primarily in Scenarios B and C. Scenario E presents a more balanced annual profile, although limited energy deficits still occur during periods of reduced photovoltaic generation.

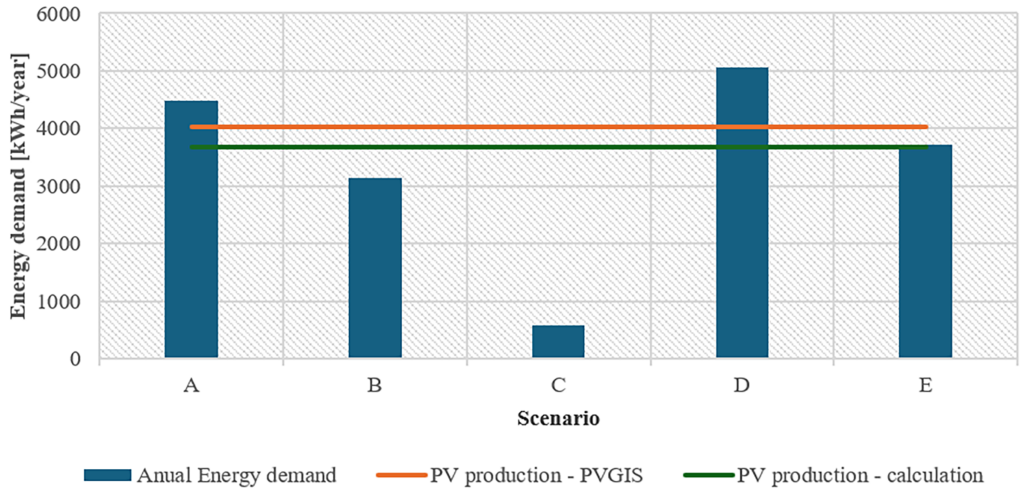


Figure 17: Comparison of annual household electricity demand and PV energy production for Scenarios A–E.

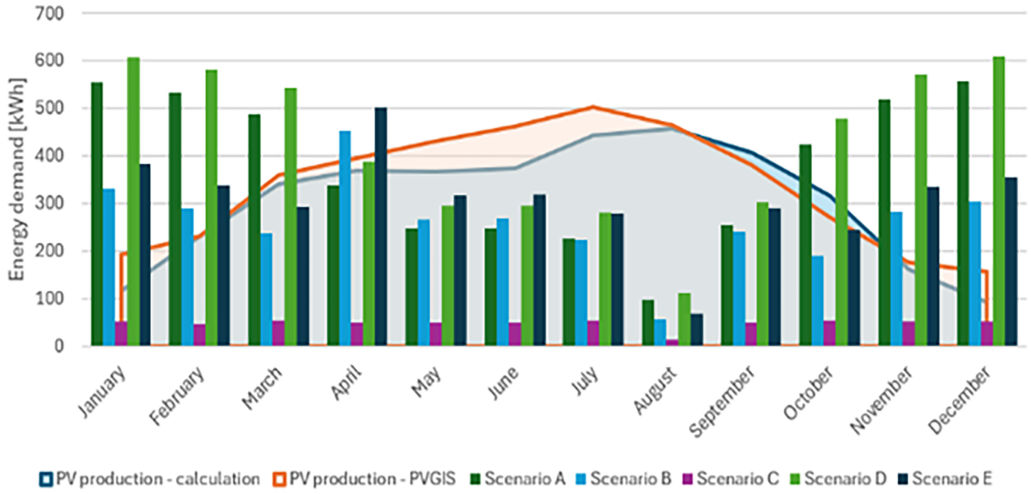


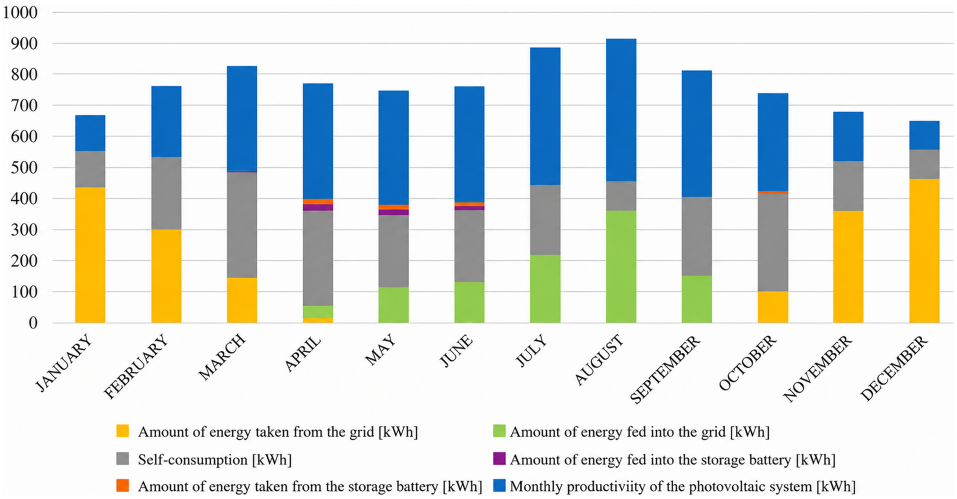
Figure 18: Monthly balance between PV energy production and household electricity demand for Scenarios A–E.

These results confirm that the effectiveness of the PV system depends not only on the annual energy balance but also on the temporal alignment between electricity generation and demand. Representative daily PV–demand balance profiles for selected winter and summer months are reported in Appendix A.2.

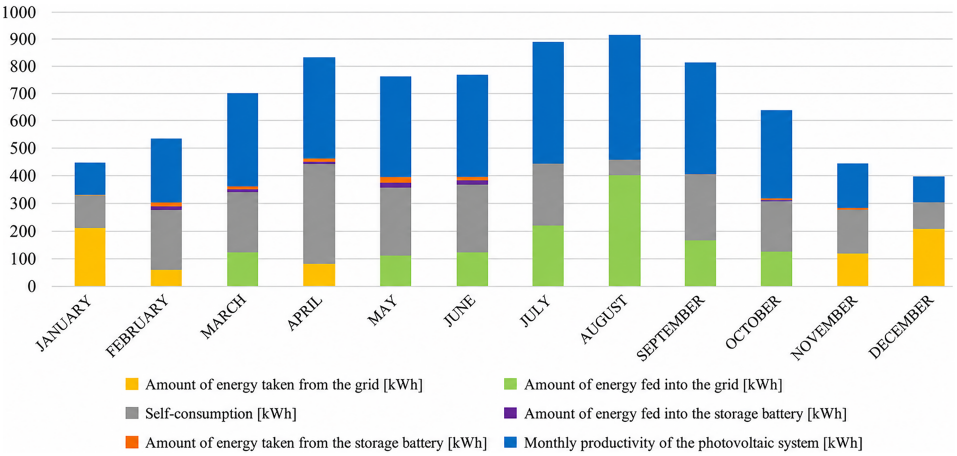
5.2 Energy Management of the Hybrid PV System

The monthly energy-management profiles for Scenarios A–E are presented in Fig. 19a–e. The profiles describe the allocation of the available PV electricity among direct self-consumption, battery charging, grid export, battery discharge, and grid import. The results presented in this subsection refer exclusively to the hybrid configuration.

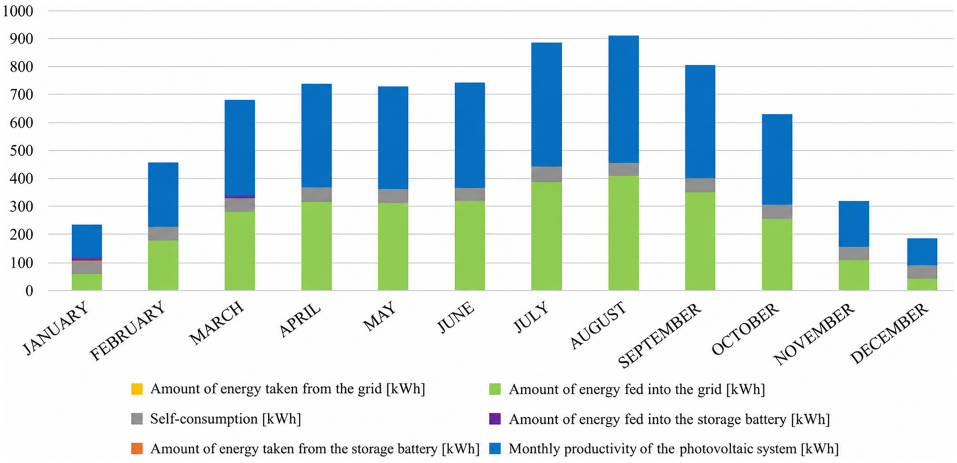
The comparison shows a clear seasonal dependence. During the winter months, grid imports represent the dominant contribution in the scenarios characterized by high system-related electricity demand, particularly Scenarios A and D. Under these conditions, most of the available PV generation is used directly by the household loads, while battery charging remains limited because little surplus energy is available.



(a)



(b)



(c)

Figure 19: (Continued)

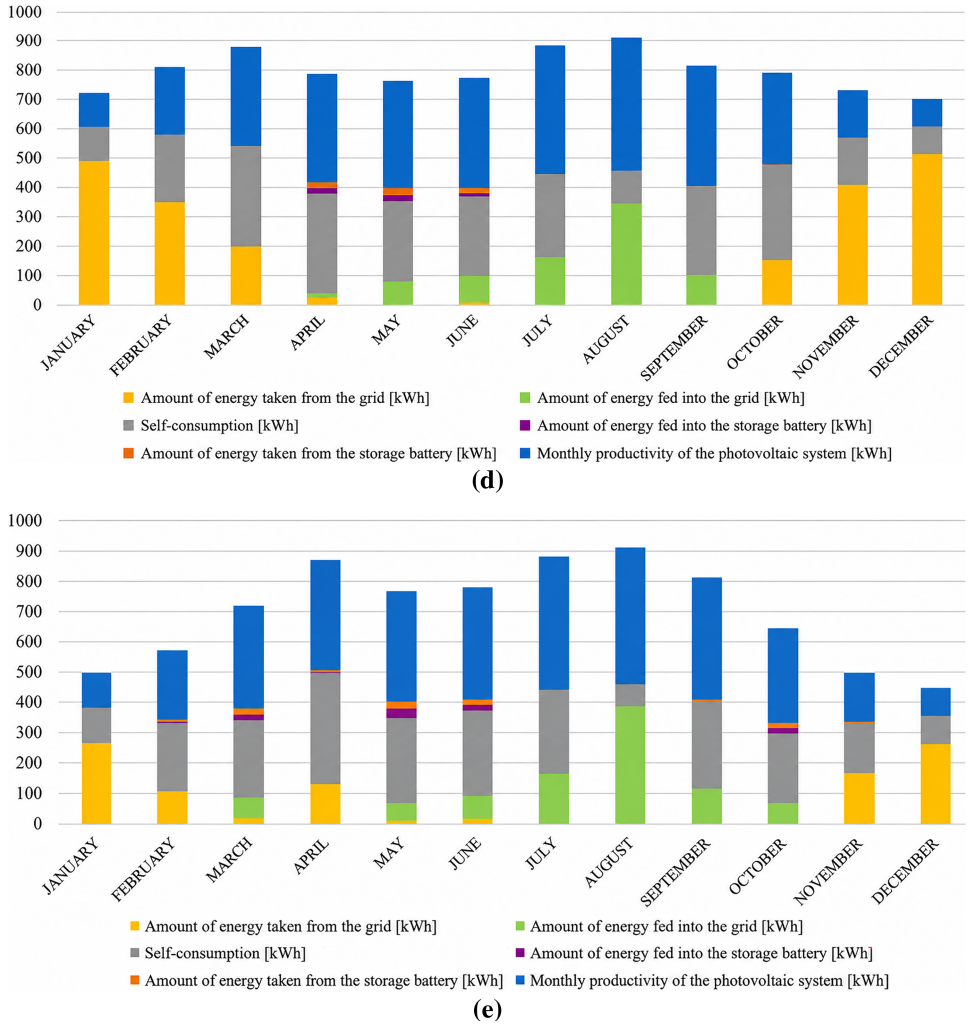


Figure 19: Comparative monthly energy-management profiles for Scenarios A–E in 2023: (**a**) Scenario A; (**b**) Scenario B; (**c**) Scenario C; (**d**) Scenario D; (**e**) Scenario E.

During spring and summer, higher PV generation improves the correspondence between production and demand. A larger share of household demand is supplied through direct self-consumption, while the available surplus is used to charge the battery. Once the available storage capacity is reached, the remaining PV electricity is exported to the grid.

Scenario C produces the greatest amount of surplus electricity because it includes household-appliance demand only. Scenario B presents a more favorable balance than Scenario A because the comprehensive retrofit reduces system-related electricity consumption. A similar difference is observed between the complete-demand configurations: Scenario E requires less grid electricity than Scenario D because of the improved envelope performance and the higher efficiency of the adopted heating and cooling systems.

The results indicate that the battery primarily mitigates short-term mismatches between PV generation and electricity demand. However, it cannot compensate for prolonged seasonal deficits because winter PV surplus is generally insufficient to support frequent battery charging. Representative daily PV–demand balance and energy-management profiles for selected winter and summer months are reported in Appendix A.2.

5.3 Preliminary Annual Performance Comparison with and without Battery Storage

To quantify the effect of battery storage on the annual performance of the photovoltaic system, a comparative assessment was carried out between the hybrid PV configuration equipped with a 5 kWh battery and an equivalent PV configuration without storage. The analysis was performed for Scenarios A, B, D, and E, while Scenario C was excluded because it represents household-appliance demand only and is already incorporated into the complete-demand scenarios. For each scenario, annual PV generation and electricity demand were assumed to be identical in both configurations, thereby isolating the effect of battery storage on the utilization of photovoltaic electricity. The comparison was based on six annual performance indicators: PV electricity utilized on site, electricity imported from the grid, electricity exported to the grid, self-consumption ratio, self-sufficiency ratio, and grid dependence. Together, these indicators provide a comprehensive assessment of the contribution of battery storage to enhancing local PV utilization, increasing energy autonomy, and reducing interactions with the electricity grid. The results of the comparison are summarized in Table 6.

Table 6: Annual energy performance comparison for Scenarios A, B, D, and E with and without 5 kWh battery storage.

Scenario	Configuration	PV Used on Site [kWh/year]	Grid Import [kWh/year]	Grid Export [kWh/year]	SCR [%]	SSR [%]	Grid Dependence [%]
A	Without battery	2595.60	1886.20	1075.78	70.70	57.91	42.09
	With battery	2646.76	1835.04	1012.01	72.09	59.06	40.94
	Change due to battery storage	+51.16	−51.16	−63.77	+1.39 pp	+1.15 pp	−1.15 pp
B	Without battery	2350.44	796.23	1320.94	64.02	74.70	25.30
	With battery	2430.33	716.34	1244.93	66.20	77.23	22.77
	Change due to battery storage	+79.89	−79.89	−76.01	+2.18 pp	+2.54 pp	−2.54 pp
D	Without battery	2820.48	2235.48	850.90	76.82	55.79	44.21
	With battery	2887.39	2168.57	793.99	78.65	57.11	42.89
	Change due to battery storage	+66.91	−66.91	−56.91	+1.82 pp	+1.32 pp	−1.32 pp
E	Without battery	2643.34	1077.48	1028.04	72.00	71.04	28.96
	With battery	2732.60	988.22	936.54	74.43	73.44	26.56
	Change due to battery storage	+89.26	−89.26	−91.50	+2.43 pp	+2.40 pp	−2.40 pp

Note: The annual values for the hybrid configuration were derived from the daily energy-management results. PV electricity used on site was calculated as annual electricity demand minus annual grid import and therefore includes both directly self-consumed photovoltaic electricity and electricity supplied to the loads through battery discharge. Grid-export values correspond to the annual values reported in Appendix B. Consequently, the reduction in grid export may differ from the reduction in grid import because battery charging and discharging are treated as distinct energy flows.

The comparison confirms that the 5 kWh battery improves the annual utilization of locally generated photovoltaic electricity across all the scenarios considered. The amount of PV electricity used on site increases by 51.16 kWh/year in Scenario A, 79.89 kWh/year in Scenario B, 66.91 kWh/year in Scenario D, and up to 89.26 kWh/year in Scenario E. At the same time, the self-consumption ratio (SCR) increases by 1.39–2.43 percentage points, while the self-sufficiency ratio (SSR) improves by 1.15–2.54 percentage points. The largest increase in self-sufficiency is observed in Scenario B, where SSR rises from 74.70% to 77.23%, corresponding to an improvement of 2.54 percentage points. Scenario E, by contrast, shows the greatest

increase in PV electricity used on site, equal to 89.26 kWh/year, together with an increase in SCR from 72.00% to 74.43% and in SSR from 71.04% to 73.44%. Scenario D exhibits the smallest improvement in self-sufficiency (+1.32 percentage points), although the amount of PV electricity used on site still increases by 66.91 kWh/year.

Battery storage also reduces the amount of electricity exchanged with the grid. Annual grid imports decrease by 51.16–89.26 kWh/year, while annual grid exports decline by 56.91–91.50 kWh/year depending on the scenario. The largest reduction in grid imports is observed in Scenario E (−89.26 kWh/year), whereas the greatest decrease in grid exports also occurs in Scenario E (−91.50 kWh/year). As a consequence, grid dependence decreases by 1.15–2.54 percentage points across the analyzed scenarios.

Nevertheless, the magnitude of these improvements remains moderate because the battery primarily mitigates short-term mismatches between photovoltaic generation and electricity demand and cannot compensate for prolonged seasonal deficits. The results therefore indicate that battery storage represents a useful complementary measure for reducing grid dependence, increasing photovoltaic self-consumption, and enhancing self-sufficiency, although its effectiveness remains strongly influenced by the temporal alignment between photovoltaic generation and household electricity demand.

The adopted 5 kWh battery should therefore be regarded as a technically feasible reference configuration rather than an optimized storage solution. Future work should address the technical and economic optimization of storage capacity by considering usable depth of discharge, round-trip efficiency, control strategy, electricity tariffs, replacement costs, and the seasonal availability of PV surplus.

6 Results and Discussion

The annual PV balance, self-consumption, grid interaction, and battery operation indicators for the five analyzed scenarios are summarized in Appendix B. Based on the scenarios analyzed, a comparison was carried out in terms of self-sufficiency over the year 2023.

This comparison highlights differences in energy-management strategies and in the ability of the PV system to meet local electricity demand. The self-sufficiency rate was calculated as the ratio between the photovoltaic energy directly consumed on-site and the total energy demand, according to Eq. (12) [4,5]:

$$SS = \frac{EPV_{self-consumed}}{E_{demand}} \cdot 100 \tag{12}$$

where $\boldsymbol{SS}$ is the self-sufficiency rate [%], $\boldsymbol{EPV_{self-consumed}}$ is the amount of photovoltaic energy directly used by the load, and $\boldsymbol{E_{demand}}$ is the total energy demand during the considered period.

As shown in Fig. 20, photovoltaic self-sufficiency varies across the analyzed scenarios and throughout the year. Scenario C reaches an annual value of approximately 99% because its limited appliance-only demand is almost entirely covered by on-site PV generation. Scenarios B and E also show favorable performance owing to the lower electricity demand associated with the comprehensive retrofit configuration, whereas Scenarios A and D remain more dependent on the grid, particularly during winter. All scenarios reach full monthly demand coverage in July and August, while the lowest self-sufficiency values occur in January and December because reduced solar availability coincides with higher system-related electricity demand.

These results suggest that Scenario C provides the most favorable case in terms of self-sufficiency, because its limited electricity demand is almost entirely covered by photovoltaic energy. However, in line with the approach proposed by Viti et al. [4] and Ciocia et al. [7], this result must be interpreted together with the self-consumption indicator. A high self-sufficiency rate does not necessarily imply that most of the photovoltaic production is used locally; it only shows the share of the load covered by on-site PV generation.

This distinction is confirmed by the behavior of the analyzed scenarios: Scenario C reaches an annual self-sufficiency of approximately 99%, but it also presents the lowest self-consumption rate, equal to 15.48%, because most of the PV production exceeds the local demand and is injected into the grid. Conversely, Scenario D achieves the highest self-consumption rate, equal to 76.82%, since its higher electricity demand allows a larger share of PV production to be directly used on-site. Therefore, Scenario C can be considered a useful upper-bound case for demand coverage, but not the most representative configuration of the overall energy behavior of the apartment.

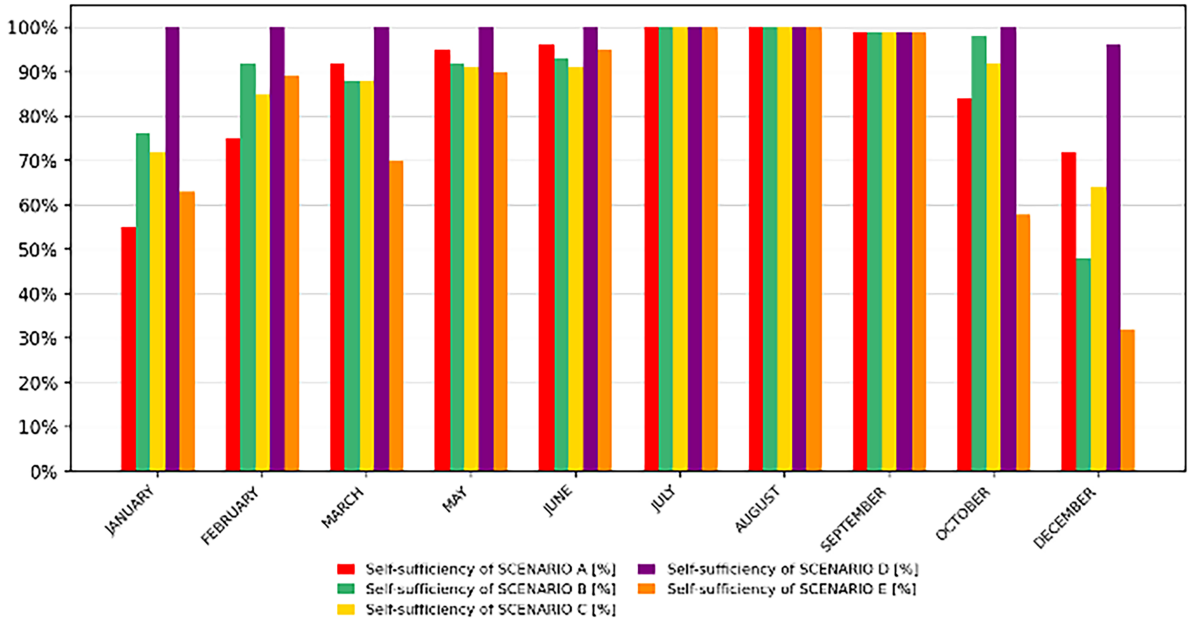


Figure 20: Monthly photovoltaic self-sufficiency of the five analyzed scenarios relative to total electricity demand.

Grid imports were analyzed to complement the self-sufficiency assessment and quantify the residual dependence of each scenario on the external electricity supply. The corresponding monthly values for 2023 are reported in Table 7.

Table 7: Monthly electricity imported from the grid for the five analyzed scenarios in 2023 [kWh].

Month	Scenario A [kWh]	Scenario B [kWh]	Scenario C [kWh]	Scenario D [kWh]	Scenario E [kWh]
JANUARY	438.20	214.43	1.87	489.88	266.11
FEBRUARY	302.92	60.78	0.00	349.86	106.68
MARCH	147.33	11.98	0.00	201.48	21.53
APRIL	15.87	82.71	0.00	28.77	130.98
MAY	0.00	6.37	0.00	4.12	12.54
JUNE	4.84	10.85	0.00	11.92	19.12
JULY	0.00	0.00	0.00	0.00	0.00
AUGUST	0.00	0.00	0.00	0.00	0.00
SEPTEMBER	0.00	0.00	0.00	0.00	0.00
OCTOBER	102.70	0.00	0.00	156.70	0.00
NOVEMBER	359.50	118.65	0.00	410.47	169.00

(Continued)

Table 7 (continued)

Month	Scenario A [kWh]	Scenario B [kWh]	Scenario C [kWh]	Scenario D [kWh]	Scenario E [kWh]
DECEMBER	463.69	210.57	0.00	515.38	262.25
TOTAL	**1835.04**	**716.34**	**1.87**	**2168.57**	**988.22**

As illustrated in Fig. 21, Table 7 confirms the differences identified through the self-sufficiency analysis. Scenario C requires only 1.87 kWh/year from the grid, whereas Scenarios B and E limit annual imports to 716.34 and 988.22 kWh/year, respectively. The highest grid dependence occurs in Scenarios A and D, which require 1835.04 and 2168.57 kWh/year from the grid. Imports are concentrated mainly in January, February, November, and December, while they are absent in all scenarios from July to September.

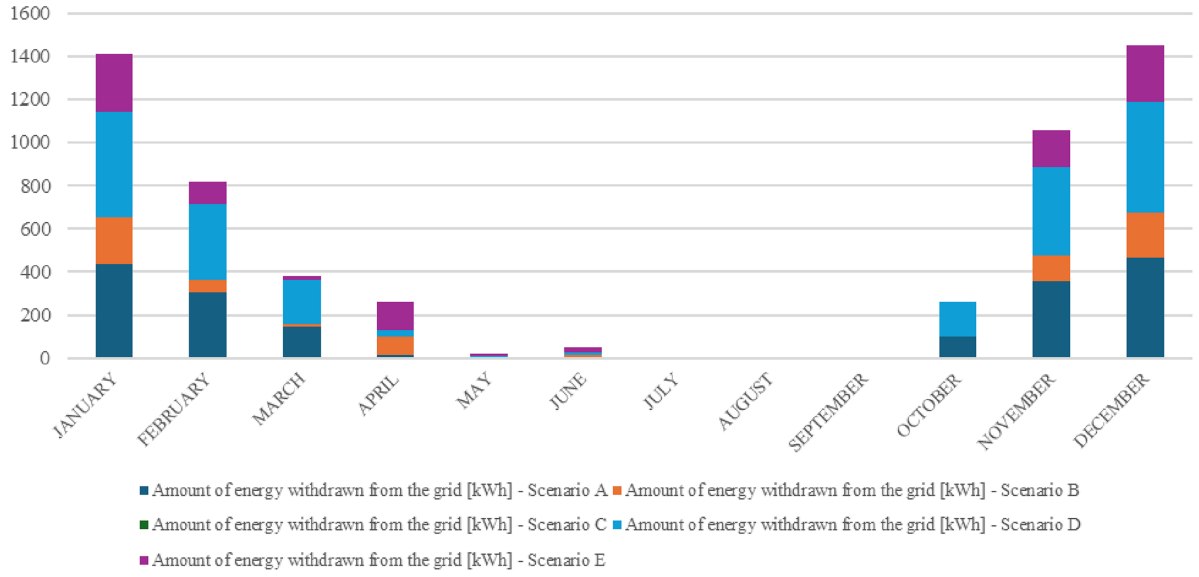


Figure 21: Monthly electricity imported from the grid for the five analyzed scenarios in 2023.

This seasonal behavior is consistent with the findings of Barone et al. [5] and Lazaroiu and Roscia [10], who emphasize that effective local energy sharing depends not only on annual renewable generation but also on the temporal correspondence among production, consumption, and available flexibility resources. The present results further show that battery storage can mitigate short-term mismatches but cannot compensate for prolonged winter deficits.

The electricity exported to the grid represents the portion of PV generation that is not used locally and could potentially support collective self-consumption within an REC. This interpretation is consistent with the prosumer-based framework discussed by Zafar et al. [1] and with the role attributed to energy communities by Barone et al. [5] and Lazaroiu and Roscia [10]. However, the potential contribution to an REC depends on both the magnitude and the temporal availability of the surplus rather than on annual exported energy alone.

As reported in Table 8, Scenario C provides the largest theoretical surplus; however, it includes only household appliances and therefore does not represent the complete energy demand of the apartment. For this reason, Scenarios B and E are more representative for assessing potential participation in an REC,

because they include both HVAC-related electricity demand and domestic appliances. This interpretation is consistent with Liu et al. [3], who underline the importance of household appliance operation and demand-side characterization in smart-home energy management. Fig. 22 provides a graphical comparison of the surplus electricity available under the five scenarios.

Table 8: Monthly electricity exported to the grid for the five analyzed scenarios in 2023 [kWh].

Month	Scenario A [kWh]	Scenario B [kWh]	Scenario C [kWh]	Scenario D [kWh]	Scenario E [kWh]
JANUARY	0.00	1.00	61.42	0.00	0.00
FEBRUARY	0.00	0.18	183.05	0.00	0.00
MARCH	0.00	109.88	285.92	0.00	67.18
APRIL	38.27	0.00	319.58	12.28	0.00
MAY	114.56	107.31	317.13	78.22	57.35
JUNE	127.65	113.81	324.08	88.86	73.45
JULY	218.29	219.73	388.85	163.42	164.87
AUGUST	360.48	401.19	444.11	347.18	387.89
SEPTEMBER	152.76	165.69	357.71	104.02	116.96
OCTOBER	0.00	125.50	261.46	0.00	68.85
NOVEMBER	0.00	0.62	109.30	0.00	0.00
DECEMBER	0.00	0.00	41.48	0.00	0.00
TOTAL	**1012.01**	**1244.93**	**3094.09**	**793.99**	**936.54**

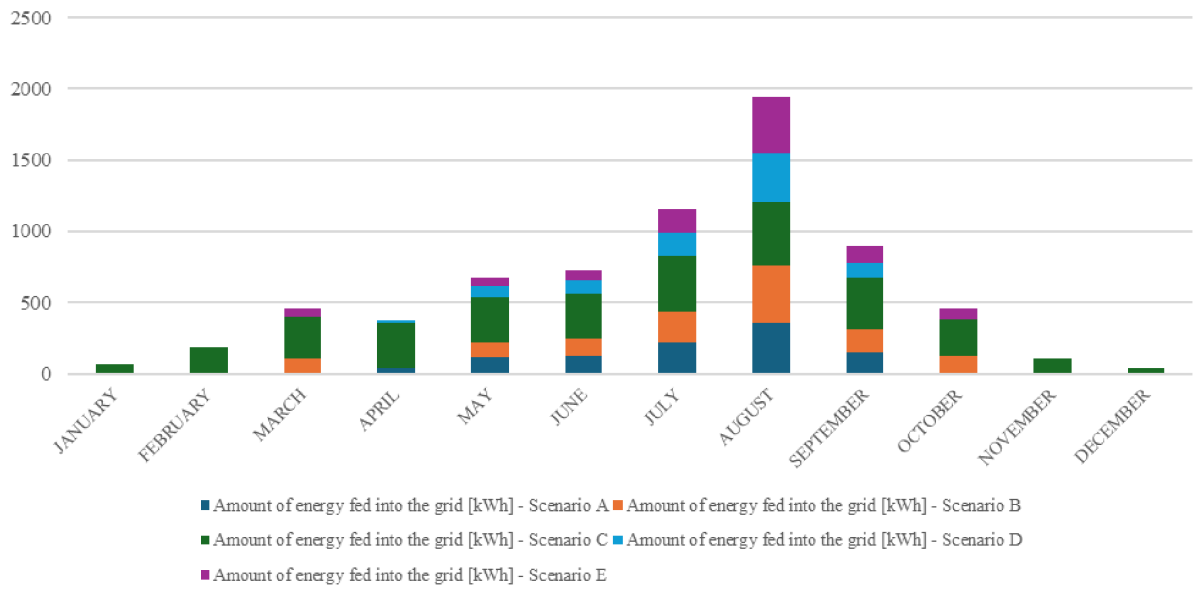


Figure 22: Monthly electricity exported to the grid for the five analyzed scenarios in 2023.

The energy fed into the grid represents a key parameter for participation in an REC, because it identifies the amount of locally produced renewable electricity that could be made available for sharing. Scenarios characterized by high photovoltaic surplus can contribute to collective self-consumption and to a more flexible local energy management strategy, in line with the role of energy communities discussed in [5,10].

In this context, Scenario C shows the highest annual grid injection, equal to 3094.09 kWh/year, followed by Scenario B with 1244.93 kWh/year and Scenario A with 1012.01 kWh/year. Nevertheless, Scenario C should be interpreted as a theoretical upper-bound case, since it includes only household appliances and does not represent the complete energy demand of the apartment. Conversely, Scenarios B and E provide a more realistic evaluation of the potential for participation in an REC, because they include both system-related electricity demand and domestic appliances. This distinction is important because the suitability of a residential unit for energy sharing depends not only on the amount of surplus electricity, but also on the completeness of the demand profile and on the seasonal availability of shareable renewable energy.

These results indicate that the potential contribution to an REC depends not only on the annual surplus injected into the grid, but also on the realism of the demand profile, the seasonal availability of photovoltaic production, the level of self-consumption and the amount of electricity still withdrawn from the grid. During the summer months, photovoltaic production is sufficient to cover the local demand in all scenarios and to generate surplus electricity. Conversely, during the winter months, grid withdrawals remain significant in the scenarios characterized by higher demand, due to lower solar availability and a stronger mismatch between production and consumption. This confirms that REC participation should be evaluated through a combined assessment of self-sufficiency, self-consumption, grid withdrawals, battery operation and surplus availability, rather than through annual PV production alone. Compared with studies addressing the energy transition at building or community scale, such as Aruta et al. [2], and with techno-economic analyses comparing individual self-consumption and energy community configurations, such as Viti et al. [4], the novelty of the present work lies in applying this integrated assessment to a single apartment within a condominium context. The proposed approach combines energy diagnosis, retrofit scenarios, photovoltaic production assessment, battery operation, grid interaction and REC participation potential under realistic constraints, including limited installation surface, seasonal mismatch between production and demand, and the need to represent household energy uses through complete demand scenarios. This makes the methodology applicable to similar urban condominium buildings, where technical and spatial constraints can significantly affect the real feasibility of photovoltaic self-consumption and renewable energy sharing.

Nevertheless, the quantitative results are specific to the climatic, geometric, technical, and occupancy conditions of the selected case study. Household-appliance profiles were reconstructed from representative use assumptions rather than measured smart-meter data, while the 5 kWh battery was adopted as a technically plausible reference configuration rather than as the result of a complete techno-economic optimization. In addition, the analysis is scenario-based and does not constitute an experimental validation of the operating PV system. These limitations restrict the direct generalization of the numerical results but do not affect the transferability of the proposed methodology, which can be applied to other residential buildings by updating the input data and operating assumptions.

7 Conclusion

This study proposes an integrated methodology for evaluating photovoltaic self-consumption, energy self-sufficiency, storage operation, grid interaction, and renewable energy-sharing potential for a condominium apartment. The framework combines building energy diagnosis, envelope and system retrofit measures, site-specific photovoltaic production, residential demand profiles, and battery operation, thereby addressing the principal constraints of urban applications, including limited installation space, local shading, seasonal demand variability, and temporal mismatch between generation and consumption.

The results show that the performance of a residential photovoltaic system cannot be evaluated solely through annual production or the aggregate balance between generation and demand. Building efficiency,

system performance, electricity-demand profiles, storage operation, and site-specific solar conditions jointly determine the interaction between the apartment, the photovoltaic system, and the electricity grid.

The comparison among the demand scenarios confirms that self-consumption and self-sufficiency describe different aspects of system performance. Higher electricity demand may increase the proportion of photovoltaic energy used on-site, whereas lower demand may reduce grid dependence while leaving a larger share of production available for export. The preferred configuration therefore depends on whether the main objective is to maximize local renewable-energy use, increase energy self-sufficiency, or make surplus electricity available for collective sharing.

The analysis also demonstrates the importance of using time-resolved production and demand profiles. Favorable annual energy balances did not prevent grid withdrawals when photovoltaic generation and electricity demand occurred at different times. In particular, summer surpluses could not offset winter deficits when space-heating demand was significant. Battery storage can reduce short-term mismatches, but it cannot compensate for prolonged seasonal differences between generation and consumption. The comparison between PVGIS estimates and the site-specific calculation indicates that local shading and installation conditions can materially influence the expected photovoltaic output. Standardized simulation tools remain useful for preliminary assessments, but their results should be complemented by analyses of obstacle geometry and local constraints in dense urban and condominium contexts. Conservative production estimates provide a more reliable basis for system sizing and the evaluation of grid exchanges. From a practical perspective, the findings support the coordinated planning of building retrofit measures, efficient heat-pump systems, photovoltaic generation, and energy-management strategies. Reducing heating and cooling requirements improves the ability of a limited rooftop photovoltaic system to cover household demand, while recurring surplus production may support collective self-consumption within a Renewable Energy Community.

Since the proposed photovoltaic system is not yet operational, measured long-term data on household electricity consumption, photovoltaic production, and battery operation are not currently available. Therefore, the present study should be interpreted as a scenario-based technical feasibility assessment rather than as an experimental validation of the operational performance of an existing system. The main methodological limitations concern the reconstruction and temporal allocation of system and household loads, interannual weather variability, the assumed module operating temperature, and the simplified representation of the electrical effects of partial shading. A formal sensitivity and uncertainty analysis was outside the scope of the present study. Future work should include experimental validation through multi-year monitoring of electricity demand and photovoltaic production, together with quantitative sensitivity analyses of the main climatic and technical parameters and of the assumptions used to reconstruct the demand profiles.

The proposed methodology can support preliminary decision-making for similar apartment-scale and condominium applications by providing a structured assessment of the interaction among demand, photovoltaic generation, storage, grid exchanges, and renewable-energy sharing.

Further developments should address battery-capacity optimization, the economic assessment of investment costs and incentive mechanisms, and the extension of the analysis to multiple apartments within the same condominium or Renewable Energy Community.

Acknowledgement: The authors would like to acknowledge the support of the University of Bergamo and the National University of Science and Technology POLITEHNICA Bucharest for their scientific and institutional support. The authors also acknowledge the use of software tools and simulation platforms adopted for the energy diagnosis, photovoltaic production estimation, and energy performance assessment described in this study.

Funding Statement: The authors received no specific funding for this study.

Author Contributions: The authors confirm their contributions to this work as follows. Giuliana Daniela Foti, Alexandra Catalina Lazaroiu and Mariacristina Roscia contributed to the study conception and design, as well as to the analysis and interpretation of the results. Alexandra Catalina Lazaroiu was responsible for data collection and case-study definition. Giuliana Daniela Foti and Mariacristina Roscia carried out the energy diagnosis, photovoltaic system assessment, and scenario development. Giuliana Daniela Foti prepared the original draft of the manuscript, while Alexandra Catalina Lazaroiu and Mariacristina Roscia contributed to its review and editing. All authors reviewed and approved the final version of the manuscript.

Availability of Data and Materials: The data supporting the findings of this study are available within the article. Additional processed data related to the energy consumption profiles, photovoltaic production estimates, and scenario calculations are available from the Corresponding Author, upon reasonable request.

Ethics Approval: Formal ethics approval was not required for this study, as it did not involve animal subjects, clinical experimentation, biomedical procedures, or the collection of sensitive, personal, or identifiable data. Informal information was collected by the author from acquaintances only to estimate average household appliance usage habits, specifically weekly frequency and average duration of use. No personal or identifiable data were recorded, and the information was used exclusively in aggregated form for household electricity consumption modeling. Therefore, no ethics committee approval or registration number was applicable.

Conflicts of Interest: The authors declare no conflicts of interest.

Abbreviations

PV	Photovoltaic
REC	Renewable Energy Community
kWp	Kilowatt peak
PVGIS	Photovoltaic geographical information system
HVAC	Heating, ventilation and air conditioning
EP_{gl}	Global energy performance index
A+B	Envelope retrofit package including opaque and transparent components
C	Traditional system retrofit package including condensing boiler replacement
D	Hybrid system retrofit package including air-to-air heat pump integration
E1	Electric system retrofit package integrating an air-to-water heat pump and a domestic hot water storage tank
E2	Electric system retrofit package integrating an electric boiler and an air-to-air heat pump
F	Photovoltaic system package
CO_2	Carbon dioxide
SC	Self-consumption
SS	Self-sufficiency

Appendix A Representative Daily Energy Balance Profiles for the Analyzed Scenarios

Appendix A reports selected representative daily profiles supporting the monthly electricity-demand results discussed in Section 3 and the energy-balance assessment presented in Section 5. Section 3 defines the electricity-demand profiles of the analyzed scenarios, whereas Section 5 compares household electricity demand with photovoltaic production and evaluates the resulting energy flows, including direct self-consumption, battery operation, grid withdrawal, and grid injection.

The appendix is therefore divided into two complementary parts. The first part reports the detailed daily electricity-consumption profiles for Scenarios A, B, and C, which define the system-related and household-appliance load components used to construct the complete household-demand configurations. Scenario A includes the air-to-air heat pump and the electric storage water heater, Scenario B represents the optimized

configuration based on air-to-water and air-to-air heat pumps, and Scenario C includes household-appliance demand only.

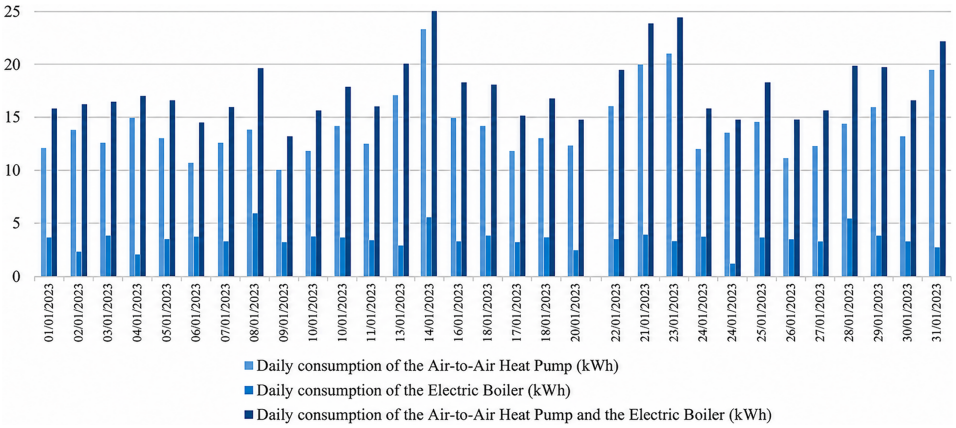
The second part reports the daily PV-demand balance and energy-management profiles for Scenarios C, D, and E. Scenario C is included as the appliance-only reference case, Scenario D represents the complete high-demand configuration obtained by combining Scenarios A and C, and Scenario E represents the optimized complete configuration obtained by combining Scenarios B and C.

Separate daily electricity-consumption profiles are not reported for Scenarios D and E because their demand profiles are already represented within the corresponding daily energy-balance figures. These figures provide a more complete representation of the interaction among household electricity demand, photovoltaic production, battery storage, grid withdrawal, and grid injection. The same representative winter and summer months are used throughout the appendix to ensure consistency and comparability among the analyzed cases.

Appendix A.1 Daily Electricity Demand Profiles

Appendix A.1.1 Scenario A

Scenario A represents the system-related electricity demand associated with the E2+F configuration, which includes an air-to-air heat pump for space heating, cooling, and dehumidification and an electric water heater for domestic hot-water production. Household-appliance loads are excluded from this scenario, consistently with the definition provided in Section 3.1. The profiles reported in Fig. A1 show the daily electricity consumption of the air-to-air heat pump, the electric water heater, and their combined demand for the selected winter and summer months. January and November represent winter operating conditions, when space-heating and domestic-hot-water requirements increase electricity demand. July and August represent summer conditions, when the heat pump is mainly used for cooling and dehumidification and the domestic-hot-water load remains comparatively limited.



(a)

Figure A1: (Continued)

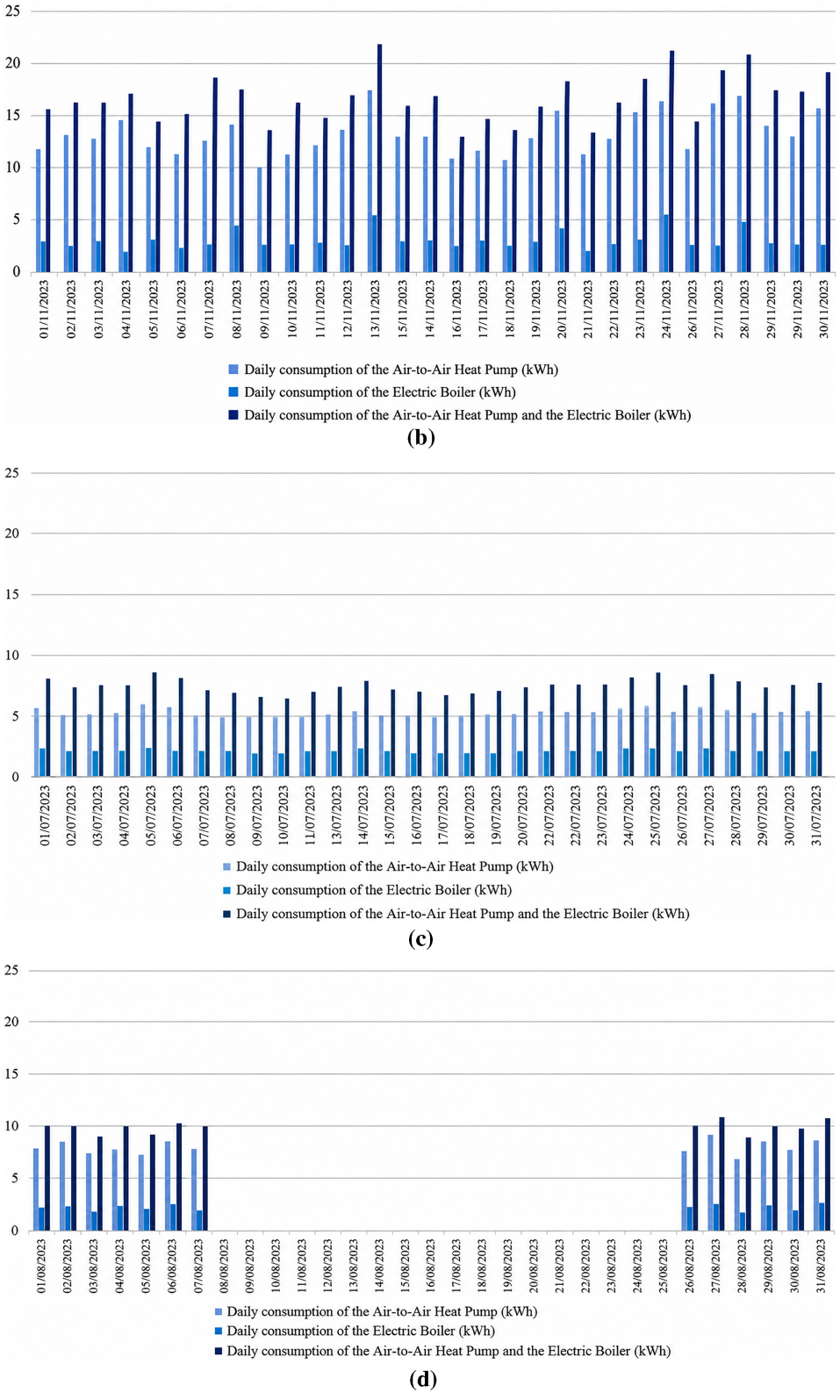


Figure A1: Daily electricity-consumption profiles for Scenario A in 2023, shown for selected representative winter and summer months. (**a**) January 2023; (**b**) November 2023; (**c**) July 2023; (**d**) August 2023.

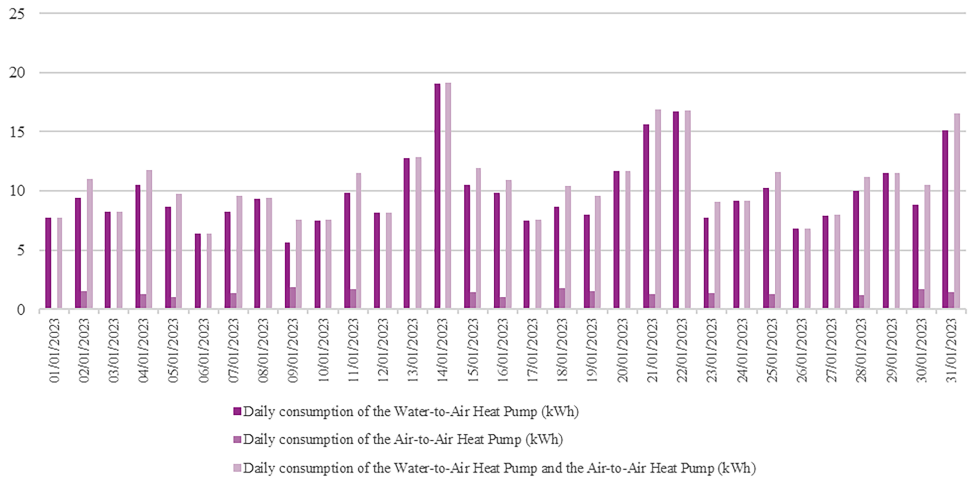
The selected daily profiles confirm the pronounced seasonal variability of Scenario A, complementing the monthly results presented in Section 3.1. January is characterized by relatively high and variable electricity demand, with several daily peaks associated with the combined operation of space-heating and domestic-hot-water systems. November shows a similarly high but more regular demand profile. In July, electricity consumption decreases and becomes comparatively stable, reflecting the predominant operation of the system for cooling, dehumidification, and domestic-hot-water production. August presents the lowest and most discontinuous profile, with electricity demand concentrated at the beginning and end of the month and no recorded consumption during the central period.

Appendix A.1.2 Scenario B

Scenario B represents the optimized system-related electricity demand associated with the A+B+E1+F configuration. The scenario includes an air-to-water heat pump for space heating and domestic-hot-water production and an air-to-air heat pump used mainly for summer cooling and dehumidification, with a limited contribution during the winter period. Household-appliance loads are excluded, consistently with the definition provided in Section 3.2.

Fig. A2 presents the daily electricity-consumption profiles for January, November, July, and August. The selected months allow the predominant winter contribution of the air-to-water heat pump to be compared with the increased summer contribution of the air-to-air heat pump, while also showing the year-round electricity demand associated with domestic-hot-water production. The same temporal framework is adopted for all scenarios to ensure direct comparability.

The selected daily profiles highlight the complementary operation of the two heat-pump systems under the optimized retrofit configuration. During January and November, electricity demand is mainly driven by the air-to-water heat pump, resulting in relatively continuous daily profiles associated with space heating and domestic-hot-water production. In July, the contribution of the air-to-air heat pump becomes more evident because of cooling and dehumidification requirements, while the air-to-water unit continues to supply domestic hot water. August shows the lowest and most discontinuous demand among the selected months. Compared with Scenario A, Scenario B exhibits lower daily consumption and a more balanced distribution of the electrical loads, reflecting the improved performance of the retrofit configuration.



(a)

Figure A2: (Continued)

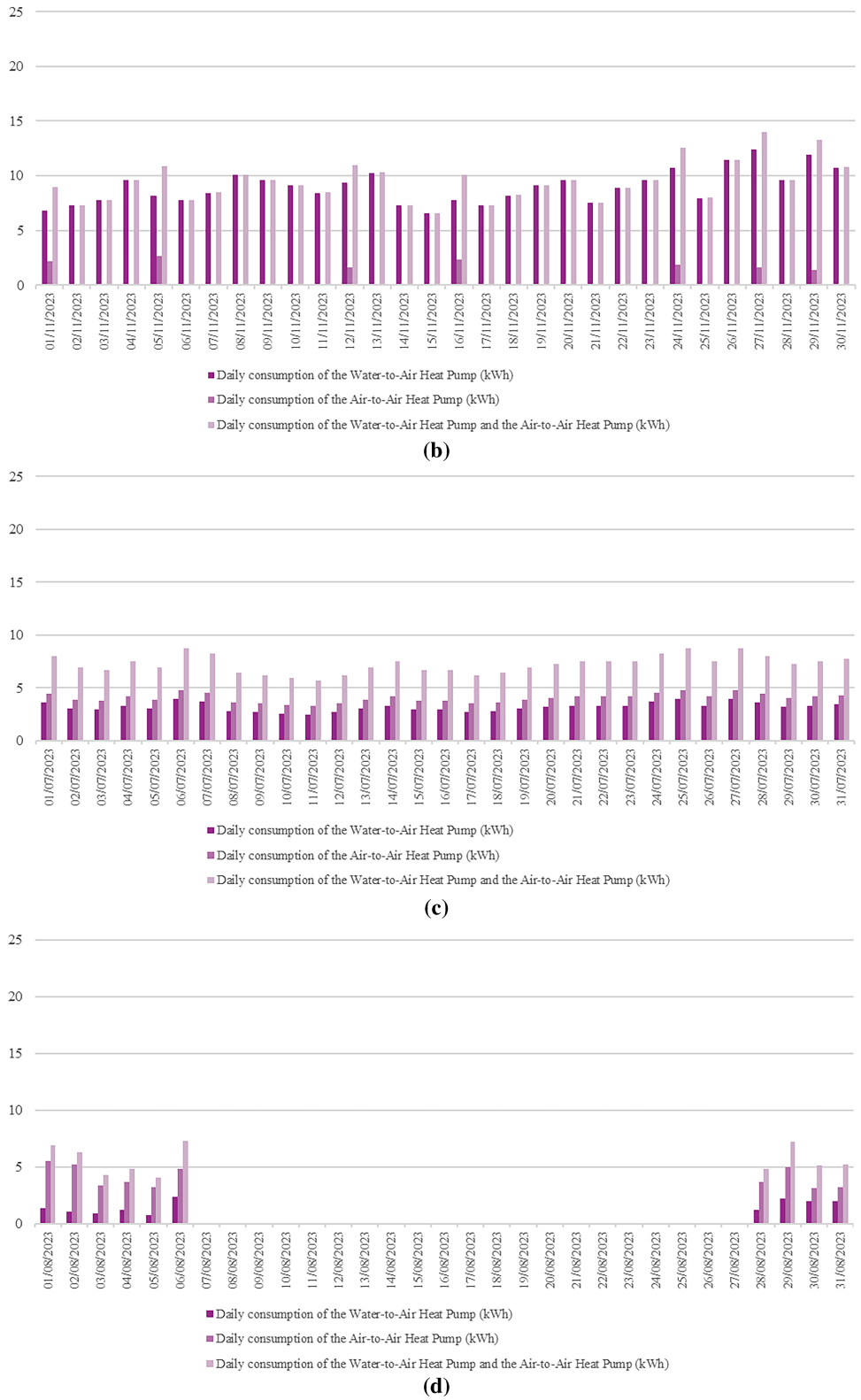


Figure A2: Daily electricity-consumption profiles for Scenario B in 2023, shown for selected representative winter and summer months. (**a**) January 2023; (**b**) November 2023; (**c**) July 2023; (**d**) August 2023.

Appendix A.1.3 Scenario C

Scenario C represents the electricity demand associated exclusively with the main household appliances considered in Section 3.3. These include the washing machine, dryer, dishwasher, refrigerator, television, and electric fan oven. Heating, cooling, dehumidification, and domestic-hot-water loads are excluded.

Fig. A3 reports the daily appliance-consumption profiles for the same four months selected for the other scenarios. January and November represent winter household-use conditions, during which the contribution of appliances such as the dryer and electric oven may become more evident. July represents a typical summer operating period, whereas August reflects the reduced household activity adopted in the reconstructed consumption profile.

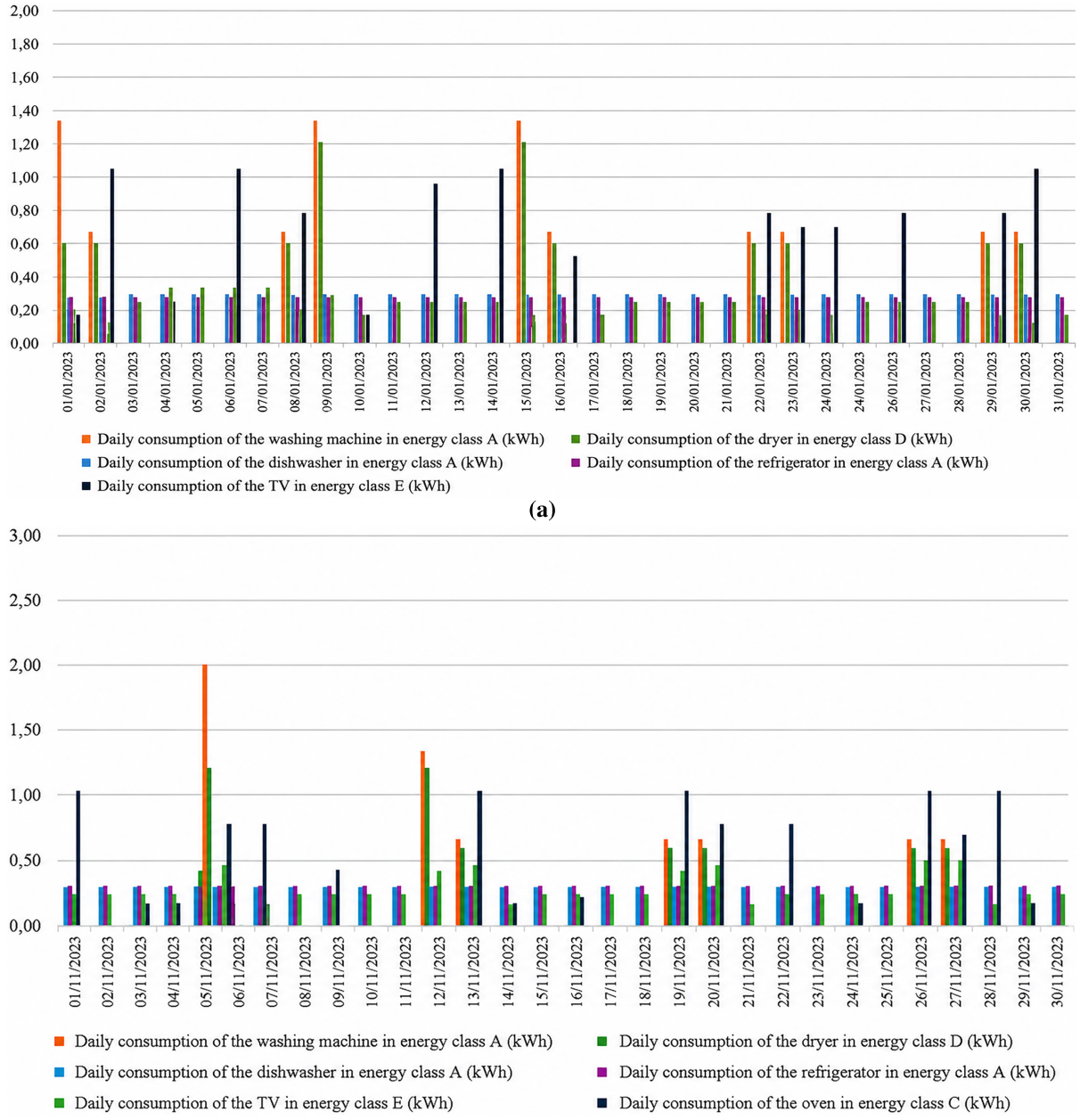


Figure A3: (Continued)

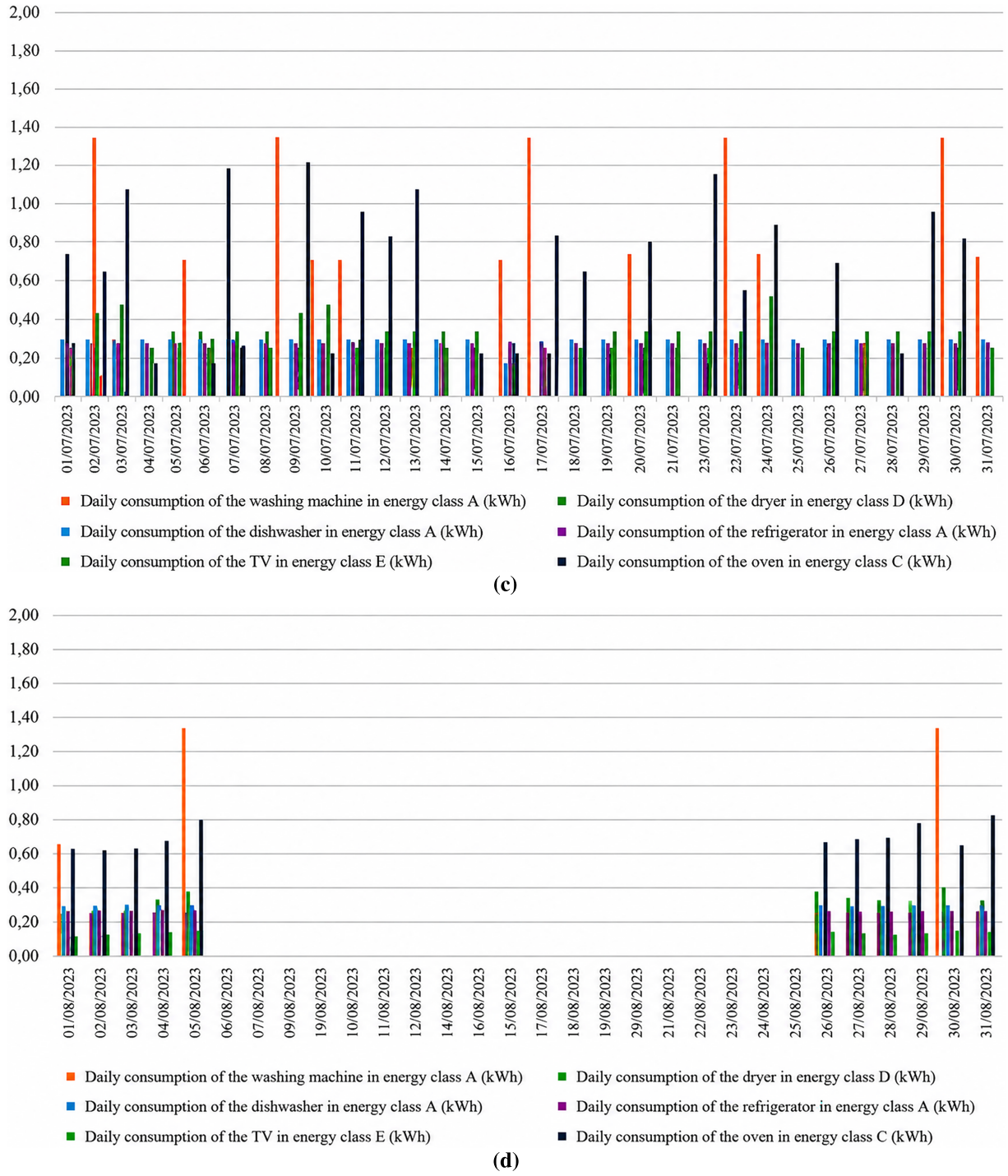


Figure A3: Daily electricity-consumption profiles for Scenario C in 2023, shown for selected representative winter and summer months. (**a**) January 2023; (**b**) November 2023; (**c**) July 2023; (**d**) August 2023.

The selected profiles show an irregular daily pattern dominated by short-duration peaks associated with the intermittent use of household appliances. January and November present more frequent variations, whereas July shows a more evenly distributed pattern. In August, consumption is concentrated at the beginning and end of the month, consistently with the reduced household activity assumed for this period.

Compared with Scenarios A and B, Scenario C has substantially lower daily electricity demand and a less pronounced seasonal variation, since its profile is determined by occupant-dependent appliance use rather than by heating, cooling, or domestic-hot-water requirements. Its contribution becomes more evident when combined with the system-related loads in Scenarios D and E.

Appendix A.2 Daily PV–Demand Balance and Energy-Management Profiles

This section presents representative daily PV–demand balance and energy-management profiles that support the monthly results discussed in Sections 5.1 and 5.2. January and August were selected to represent typical winter-deficit and summer-surplus operating conditions, respectively.

For each scenario, the PV–demand balance was evaluated by comparing the daily photovoltaic generation estimated using the analytical method with the corresponding daily household electricity demand. Positive values indicate a photovoltaic surplus, whereas negative values indicate an energy deficit.

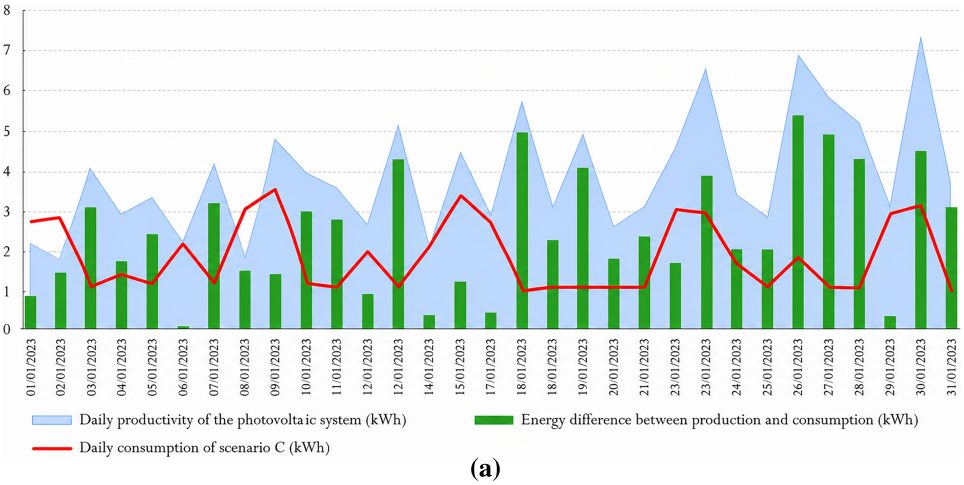
The energy-management profiles refer to the hybrid photovoltaic configuration equipped with a 5 kWh battery and illustrate the distribution of PV electricity among direct self-consumption, battery charging, grid export, battery discharge, and grid import.

Scenarios C, D, and E were selected as representative cases for the daily assessment, representing appliance-only demand, complete household demand under the reference configuration, and complete household demand under the optimized retrofit configuration, respectively. Scenarios A and B are not reported separately because their system-related electricity-demand profiles are already incorporated into the complete-demand configurations represented by Scenarios D and E.

Appendix A.2.1 Scenario C

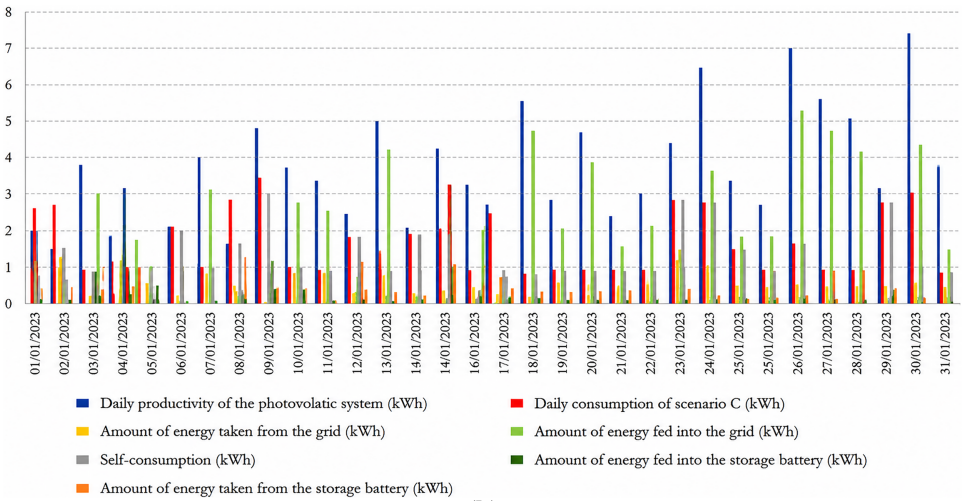
As the lowest-demand case among the analyzed scenarios, Scenario C highlights the interaction between appliance-related electricity consumption and photovoltaic generation, resulting in frequent periods of photovoltaic surplus. The representative January and August profiles are shown in Fig. A4.

In January, the comparatively low appliance demand results in the most favorable winter balance among the analyzed scenarios. Photovoltaic generation covers a relevant share of the daily demand and may also produce limited surplus electricity on favorable days. Nevertheless, grid imports remain necessary when electricity demand does not coincide with photovoltaic availability.

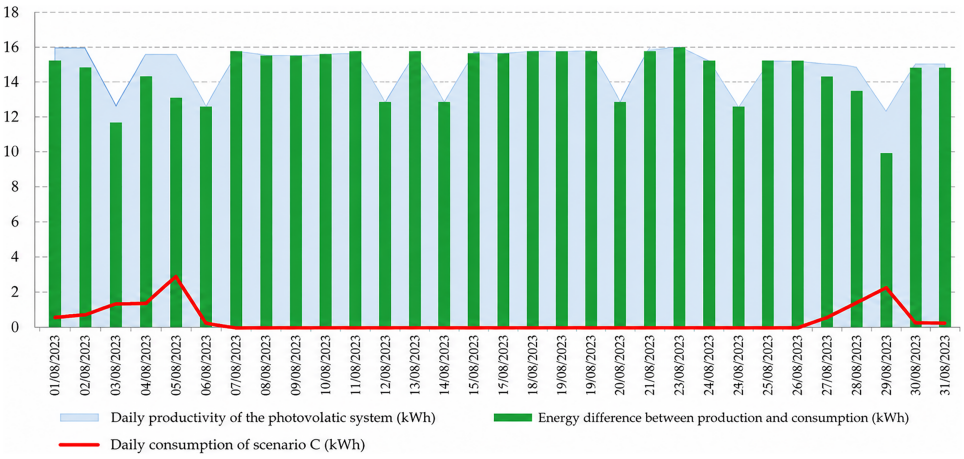


(a)

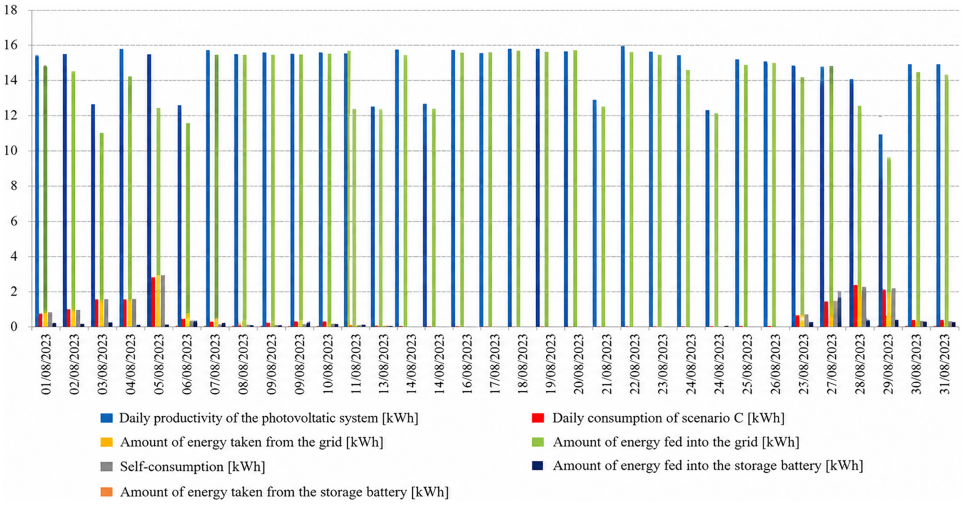
Figure A4: (Continued)



(b)



(c)



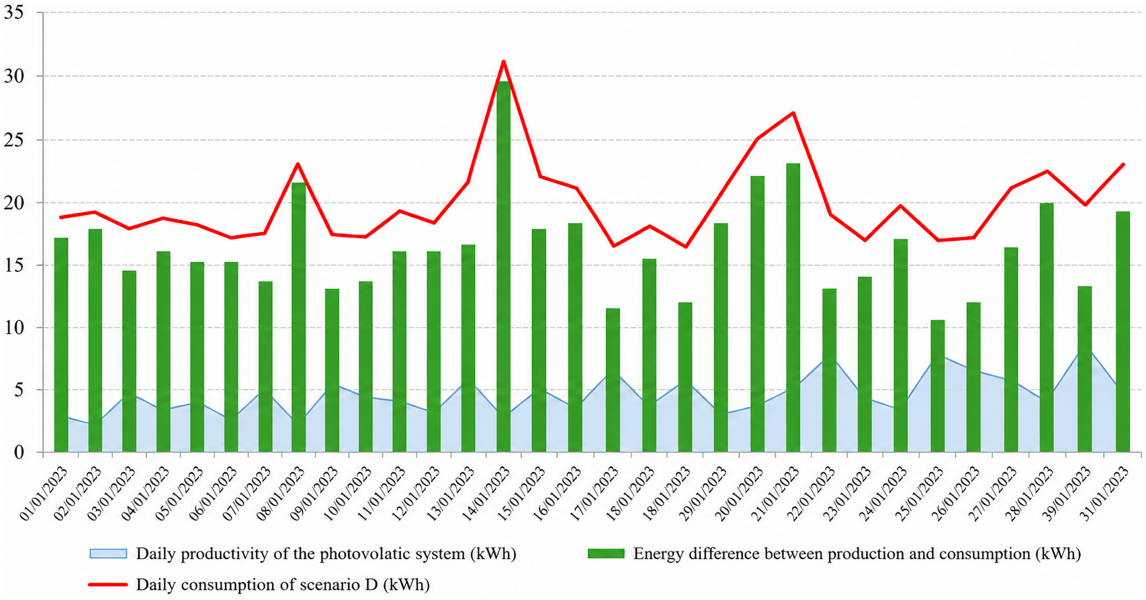
(d)

Figure A4: Representative daily PV–demand balance and energy-management profiles for Scenario C in 2023: (**a**) Daily PV–demand balance in January; (**b**) Daily energy-management profile in January; (**c**) Daily PV–demand balance in August; (**d**) Daily energy-management profile in August.

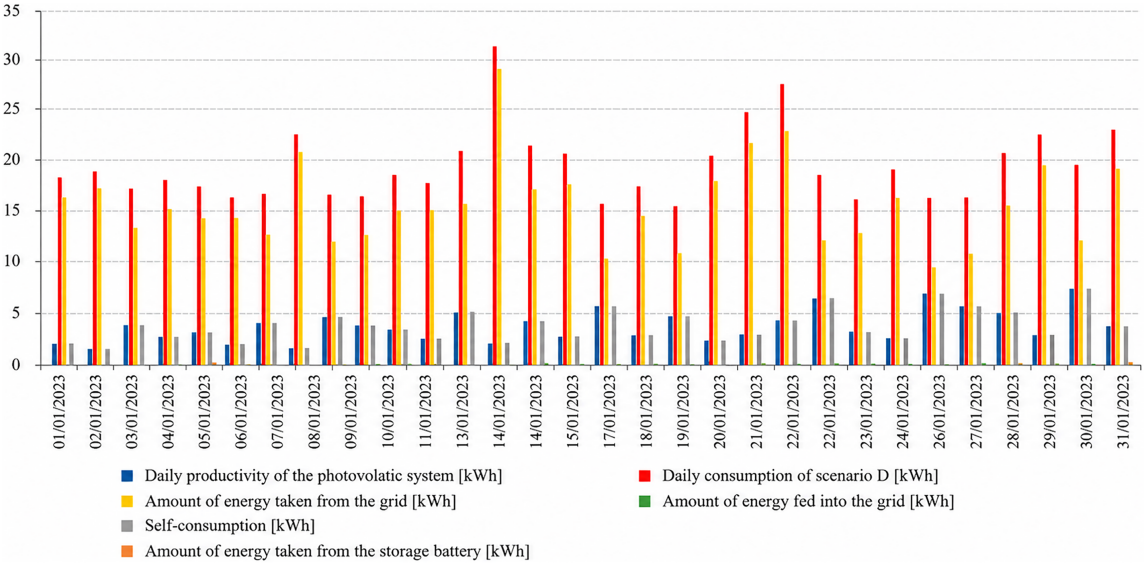
In August, photovoltaic generation substantially exceeds household-appliance demand. A portion of the generated electricity is directly self-consumed, while the remaining surplus is used to charge the battery and is subsequently exported to the grid once the available storage capacity is reached. Battery discharge mainly contributes to supplying demand outside photovoltaic-generation periods.

Appendix A.2.2 Scenario D

Scenario D represents the complete high-demand household configuration obtained by combining the system-related loads of Scenario A with the household-appliance demand of Scenario C, thereby accounting for both building-system and domestic electricity uses. The representative January and August profiles are shown in Fig. A5.

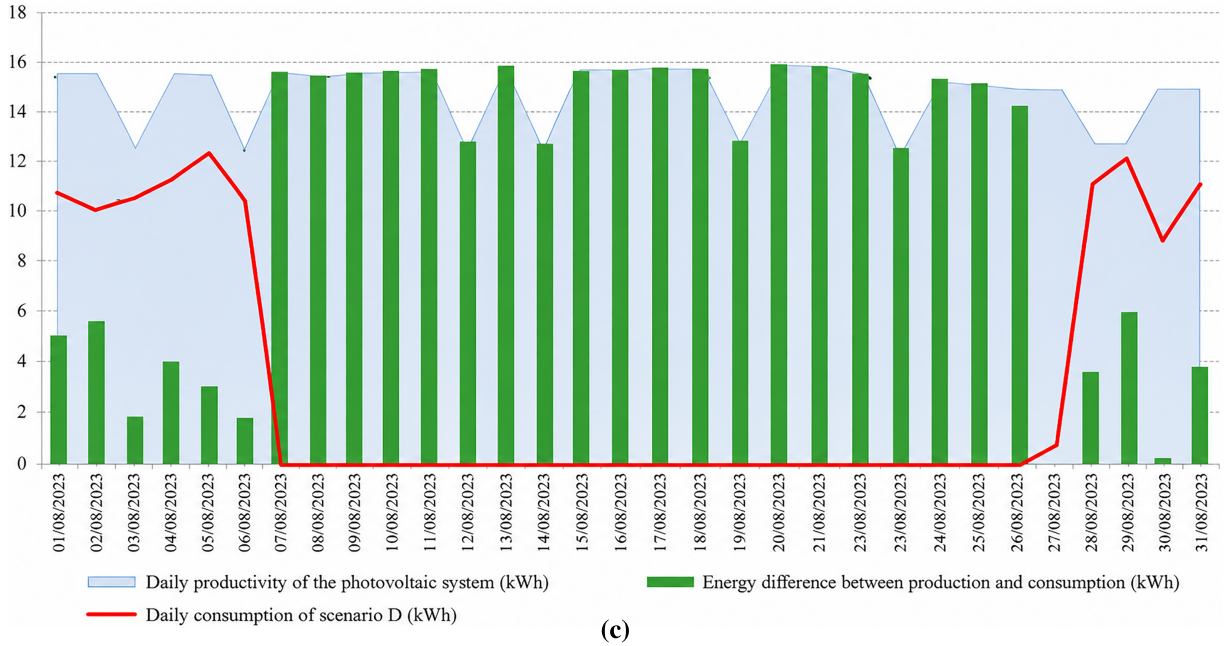


(a)

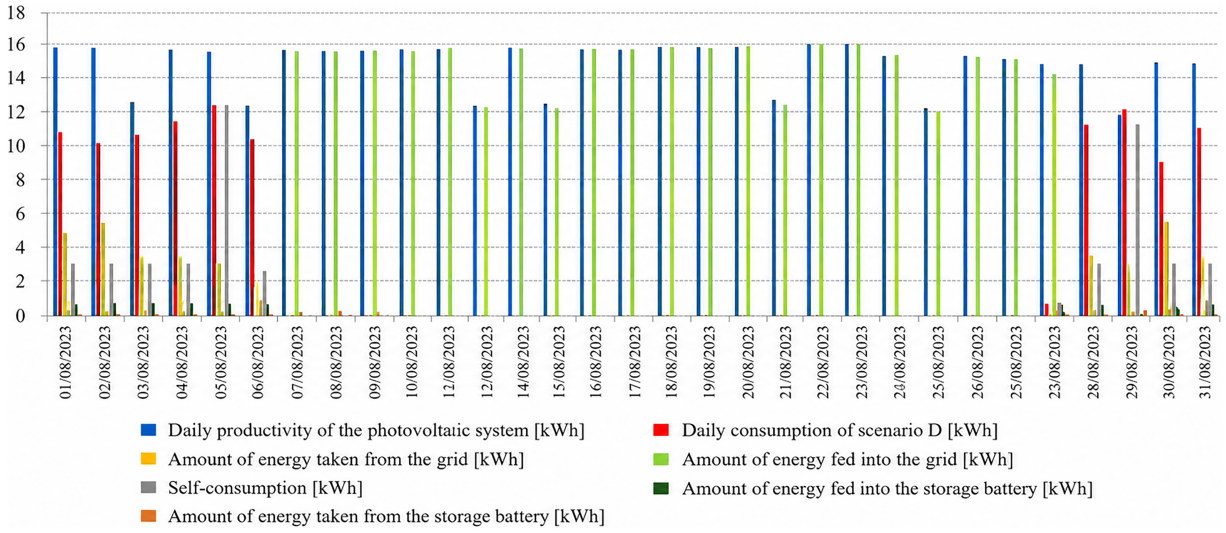


(b)

Figure A5: (Continued)



(c)



(d)

Figure A5: Representative daily PV-demand balance and energy-management profiles for Scenario D in 2023. Panels show the surplus/deficit condition and the corresponding distribution among self-consumption, battery operation, grid withdrawal, and grid injection. (**a**) Daily PV demand balance of January 2023; (**b**) Daily Energy management profiles of January 2023; (**c**) Daily PV demand balance of August 2023; (**d**) Daily Energy management profiles of August 2023.

In January, Scenario D presents the most critical daily balance because high electricity demand for space heating, domestic-hot-water production, and household appliances coincides with limited photovoltaic generation. Most of the available photovoltaic electricity is directly consumed, while only limited surplus energy is available for battery charging. Consequently, battery discharge can reduce short-duration deficits but cannot prevent substantial grid imports during prolonged periods of insufficient photovoltaic generation.

In August, the increase in photovoltaic generation and the reduction in system-related electricity demand produce frequent daily surplus conditions. Direct self-consumption supplies part of the household demand, while the remaining photovoltaic electricity is allocated to battery charging and grid export.

Nevertheless, Scenario D continues to consume a greater share of the available photovoltaic generation than the other configurations because of its higher complete-household demand.

Appendix A.2.3 Scenario E

Scenario E represents the optimized complete household configuration obtained by combining the system-related electricity demand of Scenario B with the household-appliance demand of Scenario C. Compared with Scenario D, it is characterized by lower electricity demand and a more favorable interaction with photovoltaic generation and battery storage. The representative January and August profiles are shown in Fig. A6.

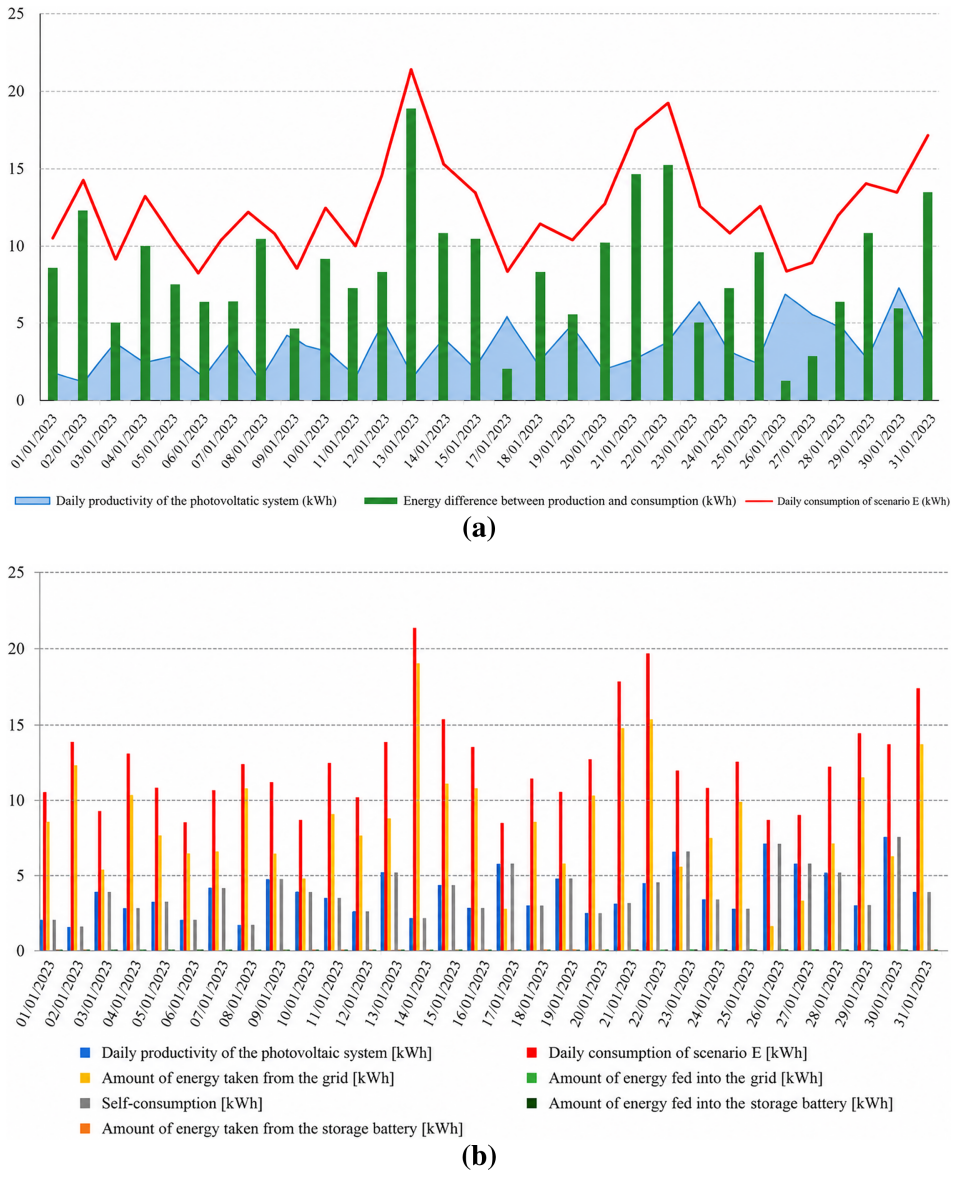
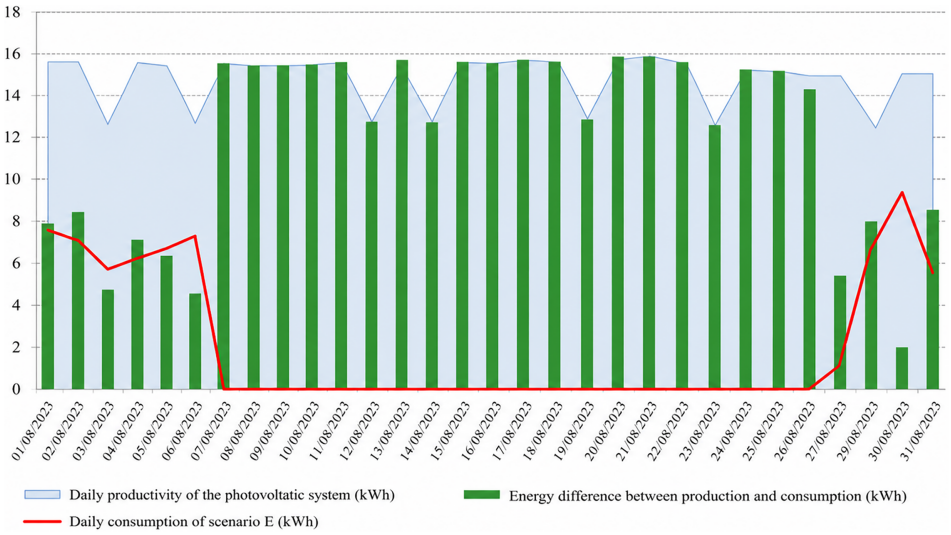
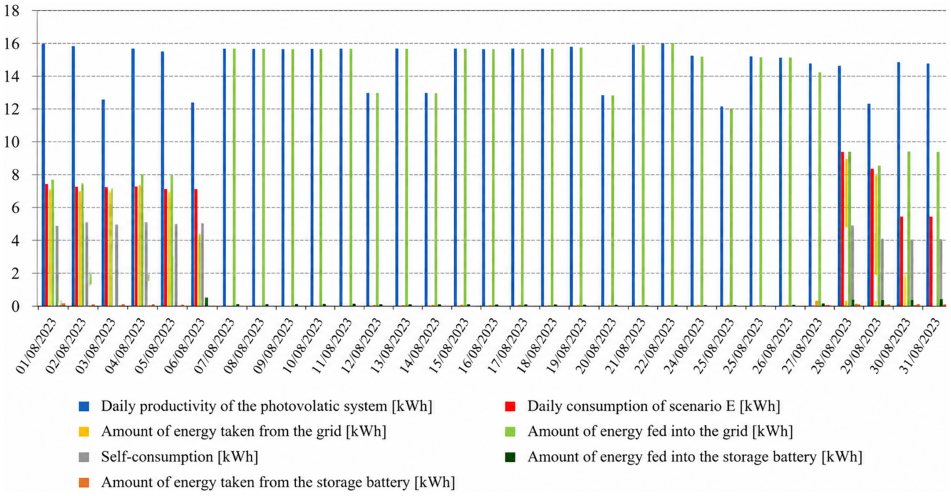


Figure A6: (Continued)



(c)



(d)

Figure A6: Representative daily PV–demand balance and energy-management profiles for Scenario E in 2023: (**a**) Daily PV–demand balance in January; (**b**) Daily energy-management profile in January; (**c**) Daily PV–demand balance in August; (**d**) Daily energy-management profile in August.

Appendix B Annual Energy Performance Indicators

Appendix B reports the annual energy-performance indicators obtained by aggregating the daily energy flows calculated for the five analyzed scenarios. The results provide a compact comparison of the annual PV–load balance, direct photovoltaic self-consumption, battery operation, and electricity exchanged with the grid. The energy-management procedure used to derive these indicators is described in Section 5.2.

For each day $\boldsymbol{d}$, the PV–load balance was calculated according to Eq. (A1):

$$\Delta \boldsymbol{E_d} = \boldsymbol{E_{PV,d}} - \boldsymbol{E_{load,d}} \tag{A1}$$

where $\boldsymbol{E_{PV,d}}$ is the daily photovoltaic production, $\boldsymbol{E_{load,d}}$ is the daily electricity demand, and $\Delta \boldsymbol{E_d}$ is the corresponding energy balance. Positive values indicate a photovoltaic surplus, whereas negative values indicate that electricity demand exceeds photovoltaic production.

The annual indicators were obtained by summing the corresponding daily energy flows over the entire year. The photovoltaic self-consumption rate was calculated according to Eq. (A2):

$$SC = \frac{EP_{V_{self-consumed}}}{E_{PV_{producion}}} \cdot 100 \quad \text{(A2)}$$

where $E_{PV,self-consumed}$ is the annual photovoltaic energy directly consumed on site and $E_{PV_{production}}$ is the total annual photovoltaic production.

The values reported in Table A1 support the comparative assessment presented in Section 6. The complete-demand scenarios show higher photovoltaic self-consumption because a larger share of the generated electricity is used locally, whereas the appliance-only scenario produces the greatest annual surplus and grid injection. These results also confirm that photovoltaic self-consumption and load coverage describe different aspects of system performance and should therefore be considered jointly.

Table A1: Annual energy performance indicators for the analyzed scenarios, including PV–load balance, PV self-consumed energy, electricity withdrawn from and injected into the grid, battery charge/discharge, and self-consumption rate.

Scenario	Scenario A	Scenario B	Scenario C	Scenario D	Scenario E
Energy demand [kWh/year]	4481.80	3146.67	574.15	5055.96	3720.82
Annual PV–load balance—calculation [kWh/year]	−810.42	524.71	3097.23	−1384.58	−49.44
Annual PV–load balance—PVGIS [kWh/year]	−459.79	875.34	3447.86	−1033.95	301.19
PV self-consumed energy [kWh/year]	2598.03	2353.36	568.23	2820.44	2626.71
Electricity withdrawn from the grid [kWh/year]	1835.04	716.34	1.87	2168.57	988.22
Electricity injected into the grid [kWh/year]	1012.01	1244.93	3094.09	793.99	936.54
Energy charged into battery [kWh/year]	58.90	77.93	8.86	61.92	94.51
Energy discharged from battery [kWh/year]	51.16	79.89	3.87	66.91	89.26
Self-consumption rate [%]	70.76	64.10	15.48	76.82	71.55

References

1. Zafar R, Mahmood A, Razzaq S, Ali W, Naeem U, Shehzad K. Prosumer based energy management and sharing in smart grid. Renew Sustain Energy Rev. 2018;82:1675–84. doi:10.1016/j.rser.2017.07.018.
2. Aruta G, Ascione F, Bianco N, Iovane T, Mastellone M, Maria Mauro G. Optimizing the energy transition of social housing to renewable nearly zero-energy community: the goal of sustainability. Energy Build. 2023;282(7):112798. doi:10.1016/j.enbuild.2023.112798.
3. Liu Y, Xiao L, Yao G, Bu S. Pricing-based demand response for a smart home with various types of household appliances considering customer satisfaction. IEEE Access. 2019;7:86463–72. doi:10.1109/ACCESS.2019.2924110.
4. Viti S, Lanzini A, Minuto FD, Caldera M, Borchiellini R. Techno-economic comparison of buildings acting as Single-Self Consumers or as energy community through multiple economic scenarios. Sustain Cities Soc. 2020;61(3):102342. doi:10.1016/j.scs.2020.102342.

5. Barone G, Buonomano A, Forzano C, Palombo A, Russo G. The role of energy communities in electricity grid balancing: a flexible tool for smart grid power distribution optimization. Renew Sustain Energy Rev. 2023;187(6):113742. doi:10.1016/j.rser.2023.113742.
6. Li S, Wang J, Zhang H, Liang Y. Solar photovoltaic power forecasting system with online manner based on adaptive mode decomposition and multi-objective optimization. Comput Electr Eng. 2024;118:109407. doi:10.1016/j.compeleceng.2024.109407.
7. Ciocia A, Amato A, Di Leo P, Fichera S, Malgaroli G, Spertino F, et al. Self-consumption and self-sufficiency in photovoltaic systems: effect of grid limitation and storage installation. Energies. 2021;14(6):1591. doi:10.3390/en14061591.
8. Frieden D, Tuerk A, Roberts J, D'Herbemont S, Gubina AF, Komel B. Overview of emerging regulatory frameworks on collective self-consumption and energy communities in Europe. In: Proceedings of the 2019 16th International Conference on the European Energy Market (EEM); 2019 Sep 18–20; Ljubljana, Slovenia. p. 1–6.
9. Ciobanu I, Lazaroiu GC, Fulginei FR. Energy community with semi-public system of EV stations, carport and batteries energy storage. In: Proceedings of the 2024 IEEE International Conference on Environment and Electrical Engineering and 2024 IEEE Industrial and Commercial Power Systems Europe (EEEIC/I&CPS Europe); 2024 Jun 17–20; Rome, Italy. p. 1–4.
10. Lazaroiu GC, Roscia M. Key elements to create renewable energy communities (REC). In: Proceedings of the 2023 12th International Conference on Renewable Energy Research and Applications (ICRERA); 2023 Aug 29–Sep 1; Oshawa, ON, Canada. p. 512–6.
11. European Union. Directive (EU) 2019/944 of the European Parliament and of the Council of 5 June 2019 on common rules for the internal market for electricity. Brussels, Belgium: European Union; 2019 [cited 2025 Jan 1]. Available from: https://eur-lex.europa.eu/legal-content/EN/TXT/PDF/?uri=CELEX:32019L0944.
12. Jung N, Moula ME, Fang T, Hamdy M, Lahdelma R. Social acceptance of renewable energy technologies for buildings in the Helsinki Metropolitan Area of Finland. Renew Energy. 2016;99:813–24. doi:10.1016/j.renene.2016.07.006.
13. Foti GD, Roscia M, Sima CA. Smart modular approach models to improve the rating of energy performance certificate of residential buildings. In: Proceedings of the 2024 12th International Conference on Smart Grid (icSmartGrid); 2024 May 27–29; Setubal, Portugal. p. 148–54.
14. European Commission, Joint Research Centre. PVGIS—photovoltaic geographical information system. [cited 2025 Jan 1]. Available from: https://re.jrc.ec.europa.eu/pvg_tools/en/.
15. CED Engineering. Design and sizing of solar photovoltaic systems. [cited 2025 Jan 1]. Available from: https://www.cedengineering.com/userfiles/R08-002%20-%20Design%20and%20Sizing%20of%20Solar%20Photovoltaic%20Systems%20-%20US.pdf.
16. Duffie JA, Beckman WA. Solar engineering of thermal processes. New York, NY, USA: John Wiley & Sons; 2013.
17. Green MA. Solar cells: operating principles, technology, and system applications. Englewood Cliffs, NJ, USA: Prentice-Hall; 1982.
18. Reda I, Andreas A. Solar position algorithm for solar radiation applications. Golden, CO, USA: National Renewable Energy Laboratory; 2008. Report No.: NREL/TP-560-34302.
19. SunEarthTools. Solar elevation and shadow calculator. [cited 2025 Jan 1]. Available from: https://www.sunearthtools.com.
20. Khomami HP, Javidi MH. An efficient home energy management system for automated residential demand response. In: Proceedings of the 2013 13th International Conference on Environment and Electrical Engineering (EEEIC); 2013 Nov 1–3; Wroclaw, Poland. p. 307–12.